

General Relativistic Effects in Weak Lensing Angular Power Spectra

Nastassia Grimm,^a Jaiyul Yoo^{a,b}

^aCenter for Theoretical Astrophysics and Cosmology,
Institute for Computational Science, University of Zürich

^bPhysics Institute, University of Zürich
Winterthurerstrasse 190, CH-8057 Zürich, Switzerland

E-mail: ngrimm@physik.uzh.ch, jyoo@physik.uzh.ch

Abstract. Advances in upcoming weak lensing surveys pose new challenges for an accurate modeling of the lensing observables. With their large sky coverage, common approximations based on a flat-sky geometry cannot be used anymore to evaluate all measurable angular scales. Moreover, additional relativistic effects manifest themselves on large scales and thus need to be accounted for. In particular, the lensing magnification cannot be correctly described by the standard lensing convergence only. We present the analytical solutions for the fully-relativistic weak lensing angular power spectra, including the contribution from primordial gravitational waves. We compare the results obtained by using the Limber approximation with the precise all-sky calculations using spherical harmonics. Our numerical evaluations show that general relativistic corrections are one order-of-magnitude below cosmic variance at small scales ($l \geq 10$). At large scales ($l < 10$), however, neglecting them leads to more significant errors, especially when combined with the Limber approximation. Hence, a precise, fully-relativistic modeling is necessary at these largest scales.

Contents

1	Introduction	2
2	Weak lensing observables	4
2.1	The standard weak lensing formalism and its gauge issues	4
2.2	Weak lensing observables including all general relativistic effects	6
2.3	Weak lensing observables given a general redshift distribution	8
3	Perturbation variables and their power spectra	11
3.1	Scalar modes	11
3.2	Tensor modes	12
4	Angular power spectra with the Limber approximation	13
4.1	Angular power spectrum of the magnification	14
4.2	E- and B-mode angular power spectra	15
4.3	Cross angular power spectrum of E-modes and δD	17
5	All-sky analysis of the weak lensing angular power spectra	18
5.1	All-sky angular power spectrum of the magnification	19
5.2	All-sky E- and B-mode angular power spectra	23
5.2.1	Calculation of $a_{lm}^{\gamma\pm}(k)$	24
5.2.2	Calculation of the E- and B-mode angular power spectra	26
5.3	All-sky cross power spectrum of E-modes and δD	28
6	Numerical results for the angular power spectra	29
6.1	Angular power spectrum of the magnification	29
6.2	Shear E-mode angular power spectrum and shear-magnification cross power spectrum	34
7	Conclusion	37
A	Vector calculus identities in spherical coordinates	38
B	Calculating tensor mode contributions using the Limber approximation	39
C	Contribution of different k-vectors to the angular power spectrum	41
D	Detailed calculation of the spin-2 shear components $_{\pm 2}\gamma(\mathbf{k}, \mathbf{n})$	42

1 Introduction

Upcoming weak lensing surveys such as LSST, WFIRST or Euclid [1–3] will provide us with an exciting opportunity to learn more about cosmology and fundamental physics. In addition to a drastic improvement in measurement precision compared to the current generation, these surveys will lead to an impressive increase in the covered survey-area: for instance, Euclid will in total cover 15,000 square degrees on the sky, ten times more than KiDS [5] which is one of the most important weak lensing surveys conducted so far. However, these advances in measurements might also lead to potentially biased conclusions if not all observational and theoretical challenges are adequately addressed. From an observational point of view, a number of well-known systematics needs to be properly accounted for (see e.g. [6] for a review). At the same time, these advances also require a more precise theoretical modeling of weak lensing observables, as several approximations that have previously been sufficient need to be reconsidered.

In particular, the increase in survey area and therefore the measurability of previously inaccessible large angular scales poses new challenges for accurate theoretical computations. For previous surveys, the Limber approximation has been sufficiently accurate, giving us a relatively simple relation between 3D-matter and 2D-weak lensing power spectra based on a flat-sky geometry [7]. However, the assumption of a flat sky clearly breaks down on large angular scales. Thus, the large sky coverage of upcoming surveys poses the need for a more accurate theoretical modeling. Indeed, the impact of the Limber approximation and similar flat-sky approximations on weak lensing angular power spectra has been already investigated intensely in theoretical work (see e.g. [8–12]), concluding that they lead to errors at percent-level or above for angular multipoles $l \lesssim 40$.

However, the need for a precise consideration of the spherical sky geometry is not the only complication that arises at large scales, as this is exactly the regime where general relativistic effects manifest themselves. While the gravitational lensing itself is a relativistic phenomenon, there exist additional relativistic corrections at linear order that become significant on large scales. Indeed, it was pointed out in [13] that the standard formalism for the calculation of weak lensing observables suffers from gauge-dependencies, indicating that it does not accurately account for all physical effects. To resolve this issue, fully gauge-invariant weak lensing formalisms have been presented in [13–15]. In particular, they have shown that lensing magnification effects are not properly described by the standard lensing convergence alone. The correct description is given by the distortion in the angular diameter distance which, apart from angular distortions leading to the standard lensing convergence, also accounts for distortions in the radial direction and the observed redshift on the light cone.

Compared to cosmic shear, the lensing magnification has received less attention from both the theoretical and observational community so far. Cosmic shear measurements can be performed under the assumption that (taking intrinsic alignment aside) galaxy images would average to be perfectly circular in the absence of lensing. Magnification measurements, however, suffer from the complication that they require knowledge on the intrinsic sizes and magnitudes [16]. Therefore, while a detection of magnification effects via galaxy sizes and magnitudes is in principle possible [17], they can alone not compete with the information gained from cosmic shear measurements. However, as pointed out in [16] and [18], cosmic shear and magnification effects suffer from different systematics and thus complement each other. An analysis of both shear and magnification effects, as concluded in [18], can

lead to tighter constraints on cosmological parameters than cosmic shear only, in particular improving constraints on σ_8 and Ω_m by up to 40%. They also argue that Euclid will fulfill the requirements for accurate measurements of magnification effects, as its large survey area enables the observation of a sufficiently large galaxy sample and its low point spread function does not destroy the size information.

Given the relevance of the lensing magnification as a complementary probe to cosmic shear, a precise evaluation of the magnification angular power spectrum at large scales is vitally important to optimally interpret the data from upcoming surveys. To our best knowledge, a calculation of the magnification angular power spectrum including all general relativistic effects is missing so far. Here, we present this calculation, applying both the Limber approximation and using the spherical harmonics decomposition. While the Limber approximation has several limitations, e.g. it cannot account for the source velocity and breaks down on large scales, the spherical harmonics approach does not assume any approximation and is thus accurate on all scales. To provide a complete formalism, we also present the expressions for the shear E-mode angular power spectrum (to linear order unaffected by general relativistic effects from scalar modes) and the cross angular power spectrum between shear E-modes and the magnification (affected by the general relativistic corrections to the latter). Additionally to scalar modes we include tensor modes from primordial gravitational waves, in particular generating shear B-modes.

Once all analytical expressions are derived, we perform numerical calculations for the fully relativistic weak lensing angular power spectra. We show that, for a Euclid-like source redshift distribution, general relativistic effects lead to corrections above the percent level for large angular modes $l \leq 20$. In particular, we show that the source velocity contribution already studied in [4] only contributes to about half of this additional signal. While general relativistic contributions lead to corrections at least one order of magnitude below cosmic variance for $l \geq 10$, it gains significance for the largest scales $l < 10$. Furthermore, the error from neglecting general relativistic effects is increased when combined with the Limber approximation, showing that a precise theoretical modeling of the magnification power spectrum is vital to correctly interpret data on the largest angular scales.

This paper is structured as follows: we first revise the standard weak lensing formalism and its gauge issues in section 2. We then present the expressions for the fully relativistic weak lensing observables derived in [13–15], and describe how they are affected by a general source redshift distribution. In section 3, we revise relations for scalar and tensor mode perturbations and their power spectra that are essential for the calculations in subsequent sections. In section 4, we present the expressions for weak lensing angular power spectra using the Limber approximation and comment on its limitations. Then, in section 5, we present the precise all-sky results, carefully describing all calculational steps associated with the use of (spin-weighted) spherical harmonics. Finally, in section 6, we present our numerical evaluations. We focus on the angular power spectrum of the lensing magnification in section 6.1, as it is most affected by general relativistic effects. However, in section 6.2, we also comment on the impact of general relativistic effects and the Limber approximation on the shear E-mode angular power spectrum and the shear-magnification cross angular power spectrum. We present our summary and conclusion in section 7. In appendix A, we present some basic vector calculus identities in spherical harmonics that are used throughout this work, and in appendix B–D, we present details for the analytical calculations of weak lensing angular power spectra that are referred to where appropriate.

2 Weak lensing observables

In this section, we present the theoretical expressions for the weak lensing observables and discuss their general relativistic corrections. First, in section 2.1, we review the weak lensing formalism commonly used in literature, which we refer to as the standard formalism. Based on the detailed discussion in [13] we explain that, even if tensor modes and observer terms are accounted for, the standard formalism leads to gauge issues and does not correctly describe general relativistic effects. To account for the inaccuracies of the standard formalism, alternative weak lensing formalisms have been developed in [13–15], resulting in theoretical expressions for the weak lensing observables which we present in section 2.2. These linear-order expressions, which are gauge-invariant and include all general-relativistic effects, will serve as a basis for the analytical and numerical investigation of general-relativistic effects in weak lensing angular power spectra presented in subsequent sections. Finally, in section 2.3, we state the expressions for the weak lensing observables given an arbitrary redshift distribution of the source galaxies.

2.1 The standard weak lensing formalism and its gauge issues

Weak gravitational lensing effects are commonly described via the distortion of the angular source positions on the sky (see e.g. [19]). In this simple treatment, which we refer to as the “standard formalism”, the shape and size distortion of an infinitesimal image observed at a two-dimensional angle $\mathbf{n} = (\theta, \phi)$ and redshift z_s is described by the Jacobian matrix:

$$\mathcal{A}_{ij} = \frac{\partial \beta_i}{\partial \theta_j} = \delta_{ij} - \frac{\partial \alpha_i}{\partial \theta_j} \equiv \begin{pmatrix} 1 & 0 \\ 0 & 1 \end{pmatrix} - \begin{pmatrix} \kappa_{\text{st}} + \gamma_{1\text{st}} & \gamma_{2\text{st}} + \omega_{\text{st}} \\ \gamma_{2\text{st}} - \omega_{\text{st}} & \kappa_{\text{st}} - \gamma_{1\text{st}} \end{pmatrix}, \quad (2.1)$$

where $\boldsymbol{\alpha}$ is the two-dimensional deflection angle and $\boldsymbol{\beta} = \mathbf{n} - \boldsymbol{\alpha}$ is the unlensed angular source position. The Jacobian matrix \mathcal{A}_{ij} is usually referred to as amplification or distortion matrix. The trace κ_{st} is called the convergence and describes the magnification of images, where the subscript “st” is used to indicate that the quantity is defined as in the standard formalism. Furthermore, $\gamma_{1\text{st}}$ and $\gamma_{2\text{st}}$ are the shear components and describe the shape distortions, while the lensing rotation ω_{st} describes a change in orientation of the image on the sky.¹ The deflection angle $\boldsymbol{\alpha}$ is given by the gradient of the projected lensing potential ψ ,

$$\alpha_i = \frac{\partial \psi}{\partial \theta_i}, \quad \psi = \int_0^{\bar{r}_s} d\bar{r} \left(\frac{\bar{r}_s - \bar{r}}{\bar{r}_s \bar{r}} \right) 2\Psi(\bar{r}), \quad (2.2)$$

where $\Psi(\bar{r})$ is the Newtonian potential and \bar{r}_s is the comoving distance to the source associated to the observed source redshift z_s ,

$$\bar{r}_s = \int_0^{z_s} \frac{dz}{H(z)}. \quad (2.3)$$

Note that as a consequence of the deflection angle being a pure gradient, the lensing rotation ω_{st} is vanishing identically in the standard formalism.

The standard formalism can be extended to include the contribution of primordial gravitational waves in addition to the scalar perturbations. In this generalization, we consider

¹Note that all these weak lensing observables depend on the observed line of sight direction \mathbf{n} , and redshift z_s , which means e.g. $\kappa_{\text{st}} \equiv \kappa_{\text{st}}(\mathbf{n}, z_s)$. This is typically omitted in our notation throughout this paper, although the dependence on \mathbf{n} is sometimes written explicitly as a way of emphasizing it.

the distortion of images in a universe described by the perturbed FLRW metric

$$ds^2 = -a^2(\eta)(1 + 2\Psi)d\eta^2 + a^2(\eta)(\delta_{\alpha\beta} - 2\Psi\delta_{\alpha\beta} + 2C_{\alpha\beta})dx^\alpha dx^\beta, \quad (2.4)$$

where η is the conformal time, $a(\eta)$ is the expansion scale factor, and $C_{\alpha\beta}$ is a trace-less, divergence-less and symmetric spatial tensor. Additionally, we consider the fact that the observer's motion is perturbed. While the timelike ($u^\mu u_\mu = -1$) four-velocity of any comoving observer is given in an unperturbed FLRW universe by $\bar{u}^\mu = (1/a, 0)$, its perturbed value is given by

$$u^\mu = \frac{1}{a} (1 - \Psi, V^\alpha), \quad (2.5)$$

where V^α is the observer's peculiar velocity.

Taking tensor perturbations and the observer's peculiar motion into account, the deflection angle α can be obtained by solving the geodesic equation for the perturbed metric, while the amplification matrix is still defined as in equation (2.1). For the precise calculations of the linear-order weak lensing observables, we refer the reader to section 4 of [13] and only state the results here. For the convergence, this formalism yields

$$\kappa_{\text{st}} = \frac{3}{2}C_{\parallel o} - V_{\parallel o} + \frac{n_\alpha \delta x_o^\alpha}{\bar{r}_s} - \int_0^{\bar{r}_s} \frac{d\bar{r}}{\bar{r}} \left(2C_{\parallel} + \hat{\nabla}_\alpha C_{\parallel}^\alpha \right) + \int_0^{\bar{r}_s} d\bar{r} \left(\frac{\bar{r}_s - \bar{r}}{2\bar{r}_s \bar{r}} \right) \hat{\nabla}^2 (2\Psi - C_{\parallel}), \quad (2.6)$$

where n^α is the line-of-sight direction and $\hat{\nabla}_\alpha$ is the angular gradient for which we give explicit expressions in appendix A. Furthermore, we defined $C_{\parallel} \equiv C_{\alpha\beta} n^\alpha n^\beta$ and $C_{\parallel\alpha} \equiv C_{\alpha\beta} n^\beta$. Note that, as a further general relativistic correction, this expression (2.6) contains the contribution of perturbations at the observer position: the line-of-sight velocity $V_{\parallel o} = V_o^\alpha n_\alpha$ and the spatial shift δx_o^α of the observer, along with the tensor $C_o^{\alpha\beta}$, all affect the lensing convergence. These terms, in particular the spatial shift δx_o^α , are often absent in literature. Indeed, as we will discuss in section 2.2, the contribution of the spatial shift vanishes when all general relativistic effect are taken into account, while the peculiar velocity of the observer remains.

In the general relativistic generalization of the standard formalism, the shear components $\gamma_{i\text{st}}$, with $i = 1, 2$, are given by

$$\gamma_{i\text{st}} = \frac{1}{2}\Phi_i^{\alpha\beta} \left[-C_{\alpha\beta o} + \int_0^{\bar{r}_s} d\bar{r} \left(\frac{\bar{r}_s - \bar{r}}{\bar{r}_s \bar{r}} \right) \hat{\nabla}_\alpha \hat{\nabla}_\beta (2\Psi - C_{\parallel}) + 2 \int_0^{\bar{r}_s} \frac{d\bar{r}}{\bar{r}} \hat{\nabla}_\beta C_{\parallel\alpha} \right], \quad (2.7)$$

where $\Phi_i^{\alpha\beta}$ is defined as

$$\Phi_1^{\alpha\beta} = \theta^\alpha \theta^\beta - \phi^\alpha \phi^\beta, \quad \Phi_2^{\alpha\beta} = \theta^\alpha \phi^\beta + \phi^\alpha \theta^\beta. \quad (2.8)$$

Here, θ^α and ϕ^α are two vectors orthogonal to the line-of-sight direction n^α , with their explicit expressions given in appendix A. In this paper, the subscript i , appearing in quantities related to the shear components, will always refer to $i = 1, 2$.

Finally, the standard lensing rotation is given by

$$\omega_{\text{st}} = \left(\theta^\alpha \phi^\beta - \phi^\alpha \theta^\beta \right) \int_0^{\bar{r}_s} \frac{d\bar{r}}{\bar{r}} \hat{\nabla}_\beta C_{\parallel\alpha}. \quad (2.9)$$

Hence, while the rotation is fully vanishing for scalar modes to linear order, it obtains an apparently non-zero contribution from tensor modes, often referred to as Skrotsky effect [20].

However, as discussed below, it is simply a coordinate artifact and not an actual physical effect [13, 15].

The consideration of tensor modes and perturbations at the observer’s position provides a substantial general relativistic generalization of the simple formalism represented by equations (2.1) and (2.2). Nevertheless, an investigation of the gauge transformation properties of this extended formalism reveals that it still does not meet the requirements for future high-precision surveys: It leads to gauge-dependent results for the weak lensing observables, i.e. if a gauge different from the Newtonian gauge is chosen, expressions which are incompatible with those above can be obtained [13]. Since different gauges are physically indistinguishable, observable quantities have to be gauge-invariant, which implies that this formalism does not accurately describe the observable effects of shape magnification and distortion.

2.2 Weak lensing observables including all general relativistic effects

The standard formalism is based on the angular distortions of the source position, and, hence, on solving the geodesic equation. While the geodesic equation is naturally associated with weak lensing effects as it describes the propagation of light rays in a curved space-time, it has to be applied with caution when we relate it to the physical observables measured in the rest frame of the observer. The geodesic equation describes the light propagation in global FLRW coordinates, which do not directly refer to any observable quantity. Observables described in global coordinates would require a global observer looking at the universe as a whole and are thus not physically meaningful (see [13] for a detailed explanation). To correctly describe weak lensing quantities, observables need to be described in the observer rest frame and compared to the intrinsic size and shape in the source rest frame.

Indeed, the fact that the standard convergence given in equation (2.6) does not include all effects contributing to the magnification of images is well-known: For a more accurate description of this type of weak lensing effects, it has to be replaced with the distortion of the angular diameter distance (or, equivalently, the distortion in the luminosity distance), which additionally includes contributions from the redshift and radial distortions [21, 22]. A particularly remarkable work on cosmological weak lensing has been provided by Schmidt & Jeong in [14], where they describe a “cosmic ruler” in the source rest frame and relate it to observables. This ruler was obtained from quantities described in global coordinates applying an appropriate projection tensor. The authors have included scalar, vector and tensor modes and an explicit check of gauge invariance, and therefore provided a comprehensive formalism for magnification and shear effects. However, as the orientation of this standard ruler was not specified, the rotation was naturally absent in their calculations. This gap in the theoretical description of cosmological weak lensing was filled with the work [13], where the rotation of the image was taken into account. It was concluded that it is, in fact, fully vanishing to linear order. The Skrotsky effect given in equation (2.9) describes the rotation of an image with respect to global coordinates. To translate this into observable quantities the rotation of the local basis, parallelly transported along the line of sight, has to be taken into account, which cancels out the rotation of the image.² Another gauge-invariant formalism based on the Jacobi map has been provided in [15], where the results for the cosmological weak lensing observables of [14] and [13], including the vanishing rotation, have been confirmed with an independent method.

²Note that the lensing rotation is vanishing to linear order even when vector modes are included. However, we strongly emphasize that there is a non-vanishing higher-order rotation.

For the fully general linear-order results for the weak lensing observables, i.e. including scalar, vector and tensor modes and without choosing a certain gauge, we refer the reader to these papers. Here, we state the results adopting the Newtonian gauge and ignoring vector perturbations. To quantify magnification effects, the standard convergence κ_{st} is replaced by the distortion in the angular diameter distance,

$$\delta D = -\kappa_{\text{st}} + \delta z + \frac{\delta r}{\bar{r}_z} - \Psi - \frac{1}{2}C_{\parallel}, \quad (2.10)$$

containing the contribution of the distortion of the redshift,

$$\delta z = (\mathcal{H}\delta\eta)_o + (V_{\parallel} - \Psi)_o^s - \int_0^{\bar{r}_s} d\bar{r} (2\Psi - C_{\parallel})', \quad (2.11)$$

the distortion of the radial coordinate,

$$\delta r = n_{\alpha}\delta x_o^{\alpha} + \delta\eta_o - \frac{\delta z}{\mathcal{H}_s} + \int_0^{\bar{r}_s} d\bar{r} (2\Psi - C_{\parallel}), \quad (2.12)$$

and additional perturbations at the source position arising from correctly relating global coordinates to the rest frame of the source galaxy. Again, we want to emphasize that κ_{st} is neither observable nor gauge-invariant, and only the full quantity δD correctly quantifies measurable magnification effects. Hence, we will refer to the distortion in the angular diameter distance δD as the magnification hereafter.

Summing up all contributions, we can rewrite equation (2.10) into

$$\begin{aligned} \delta D_{\text{sc.}} = & \left(1 - \frac{1}{\bar{r}_s \mathcal{H}_s}\right) \Psi_o + \left(\mathcal{H}_o - \frac{\mathcal{H}_o}{\bar{r}_s \mathcal{H}_s} + \frac{1}{\bar{r}_s}\right) \delta\eta_o + \frac{V_{\parallel o}}{\bar{r}_s \mathcal{H}_s} + \left(\frac{1}{\mathcal{H}_s \bar{r}_s} - 2\right) \Psi \\ & + \left(1 - \frac{1}{\mathcal{H}_s \bar{r}_s}\right) V_{\parallel} - \int_0^{\bar{r}_s} d\bar{r} \left(\frac{\bar{r}_s - \bar{r}}{\bar{r}_s \bar{r}}\right) \hat{\nabla}^2 \Psi - 2 \left(1 - \frac{1}{\mathcal{H}_s \bar{r}_s}\right) \int_0^{\bar{r}_s} d\bar{r} \Psi' + \frac{2}{\bar{r}_s} \int_0^{\bar{r}_s} d\bar{r} \Psi, \end{aligned} \quad (2.13)$$

for the scalar mode contribution, and

$$\begin{aligned} \delta D_{\text{t.}} = & -\frac{3}{2}C_{\parallel o} - \frac{1}{2}C_{\parallel} + 2 \int_0^{\bar{r}_s} \frac{d\bar{r}}{\bar{r}} C_{\parallel} + \int_0^{\bar{r}_s} d\bar{r} \left(\frac{\bar{r}_s - \bar{r}}{2\bar{r}_s \bar{r}}\right) \hat{\nabla}^2 C_{\parallel} \\ & - \int_0^{\bar{r}_s} \frac{d\bar{r}}{\bar{r}} \hat{\nabla}^{\alpha} C_{\parallel \alpha} + \left(1 - \frac{1}{\mathcal{H}_s \bar{r}_s}\right) \int_0^{\bar{r}_s} d\bar{r} C'_{\parallel} - \frac{1}{\bar{r}_s} \int_0^{\bar{r}_s} d\bar{r} C_{\parallel}, \end{aligned} \quad (2.14)$$

for the tensor mode contribution. Note that the contribution of the spatial coordinate lapse,

$$\delta x_o^{\alpha} = \int_0^{\bar{\eta}_o} d\bar{\eta} V^{\alpha}(0, \bar{\eta}), \quad (2.15)$$

cancels out for the observable δD . However, the contribution of the time coordinate lapse $\delta\eta_o$ given by

$$\delta\eta_o = -v_o, \quad v^{\alpha} \equiv -V^{\alpha}, \quad (2.16)$$

where v is the velocity potential, is not vanishing. In literature, both the spatial and the temporal lapses δx_o^{α} and $\delta\eta_o$ are typically set to zero. However, this would correspond to a specific gauge-choice – the comoving-synchronous gauge – which is incompatible with

e.g. the Newtonian gauge chosen is this work, where all gauge degrees of freedom are already fixed. Hence, while the contributions of δx_o^α from κ_{st} and δr cancel out, the non-vanishing contribution of $\delta\eta_o$ needs to be considered, as omitting observer terms can break the gauge-invariance and further lead to unphysical artifacts such as infrared divergences [23].

The expressions for the shear components in the correct general relativistic description are given by

$$\gamma_i = \frac{1}{2}\Phi_i^{\alpha\beta} \left[-C_{\alpha\beta o} - C_{\alpha\beta} + \int_0^{\bar{r}_s} d\bar{r} \left(\frac{\bar{r}_s - \bar{r}}{\bar{r}_s \bar{r}} \right) \hat{\nabla}_\alpha \hat{\nabla}_\beta (2\Psi - C_\parallel) + 2 \int_0^{\bar{r}_s} \frac{d\bar{r}}{\bar{r}} \hat{\nabla}_\beta C_{\parallel\alpha} \right], \quad (2.17)$$

Comparing with equation (2.7), we see that the shear components take the same expressions as in the standard formalism for the scalar modes in the Newtonian gauge, while there is an extra contribution of tensor modes at the source position. The lensing rotation is, as already mentioned, fully vanishing to linear order,

$$\omega = 0. \quad (2.18)$$

In the subsequent sections, we will use the equations (2.10) and (2.17) for δD and γ_i to obtain the general-relativistic corrections to the weak lensing angular power spectra, given a source distribution matching the one expected for Euclid. Note that these expressions for the weak lensing observables have been derived several times with independent theoretical formalisms: the papers [13–15] fully agree on the expressions for the shear components, while for the magnification, the work in [14] only misses the contribution from the lapse η_o . All these papers present explicit checks of gauge-invariance, strongly confirming their accuracy.

2.3 Weak lensing observables given a general redshift distribution

All quantities given in the previous section are defined for a unique source redshift z_s , corresponding to an observed radial coordinate \bar{r}_s . However, weak lensing observations involve averages over many sources with a normalized distribution function $n(\bar{r})$, determining the number of galaxies dN in a radial interval $d\bar{r}$, i.e. $dN/N_{\text{tot}} = n(\bar{r})d\bar{r}$. To express the lensing observables given such as function $n(\bar{r})$, we further define the kernels

$$\begin{aligned} h(\bar{r}) &\equiv \frac{1}{\bar{r}} \int_{\bar{r}}^{\bar{r}_s} d\tilde{r} n(\tilde{r}), & g(\bar{r}) &\equiv \int_{\bar{r}}^{\bar{r}_s} d\tilde{r} \left(\frac{\tilde{r} - \bar{r}}{\tilde{r}\bar{r}} \right) n(\tilde{r}), \\ q(\bar{r}) &\equiv \int_{\bar{r}}^{\bar{r}_s} d\tilde{r} \frac{n(\tilde{r})}{\mathcal{H}(\tilde{r})\tilde{r}}, & f(\bar{r}) &\equiv \bar{r}h(\bar{r}) - q(\bar{r}) = \int_{\bar{r}}^{\bar{r}_s} d\tilde{r} \left(1 - \frac{1}{\mathcal{H}(\tilde{r})\tilde{r}} \right) n(\tilde{r}). \end{aligned} \quad (2.19)$$

Assuming that all observed galaxies are weighted equally, the observed shear components Γ_i are given by

$$\Gamma_i = \int_0^{\bar{r}_s} d\bar{r} n(\bar{r}) \gamma_i(\bar{r}), \quad (2.20)$$

where \bar{r}_s refers to the depth of the survey, i.e. the comoving distance corresponding to the highest redshift observed in the survey. This yields

$$\Gamma_i = \frac{1}{2}\Phi_i^{\alpha\beta} \left[-C_{\alpha\beta o} - \int_0^{\bar{r}_s} d\bar{r} \left(n(\bar{r})C_{\alpha\beta} + 2h(\bar{r})\hat{\nabla}_\beta C_{\parallel\alpha} \right) + \int_0^{\bar{r}_s} d\bar{r} g(\bar{r})\hat{\nabla}_\alpha \hat{\nabla}_\beta (2\Psi - C_\parallel) \right]. \quad (2.21)$$

Similarly, the measured magnification is given by

$$\Delta D = \int_0^{\bar{r}_S} d\bar{r} \tilde{n}(\bar{r}) \delta D(\bar{r}). \quad (2.22)$$

The radial depth \tilde{r}_S and the normalized redshift distribution function $\tilde{n}(\bar{r})$ can, in principle, differ from the respective quantities \bar{r}_S and $n(\bar{r})$ for the shear components. Flux magnification measurements rely only on the total flux measured and do not need to resolve the shape of the image. Thus, future surveys could potentially measure magnification up to deeper redshift than cosmic shear [24]. While we will, for simplicity, assume $\bar{r}_S = \tilde{r}_S$ and $n(\bar{r}) = \tilde{n}(\bar{r})$ for the rest of this work, we emphasize that our analytical expressions can be straight-forwardly applied to a case where these quantities differ from each other.

The above equation, combined with equation (2.10) for δD , yields the result

$$\Delta D = -K + \Delta z + \Delta r - \int_0^{\bar{r}_S} d\bar{r} n(\bar{r}) \left(\Psi + \frac{1}{2} C_{\parallel} \right), \quad (2.23)$$

where we defined the integrated quantities K , Δr and Δz as

$$\Delta r = \int_0^{\bar{r}_S} d\bar{r} n(\bar{r}) \frac{\delta r(\bar{r})}{\bar{r}}, \quad \Delta z = \int_0^{\bar{r}_S} d\bar{r} n(\bar{r}) \delta z(\bar{r}), \quad K = \int_0^{\bar{r}_S} d\bar{r} n(\bar{r}) \kappa_{\text{st}}(\bar{r}). \quad (2.24)$$

For these quantities, we obtain

$$\begin{aligned} \Delta r = & (n_{\alpha} \delta x^{\alpha} + \delta \eta)_o (h - g)(0) - (\mathcal{H} \delta \eta - V_{\parallel} + \Psi)_o q(0) + \int_0^{\bar{r}_S} d\bar{r} \frac{n(\bar{r})}{\mathcal{H} \bar{r}} (V_{\parallel} + \Psi) \\ & + 2 \int_0^{\bar{r}_S} d\bar{r} q(\bar{r}) (2\Psi' - C'_{\parallel}) + \int_0^{\bar{r}_S} d\bar{r} (h - g)(\bar{r}) (2\Psi - C_{\parallel}), \end{aligned} \quad (2.25)$$

$$\Delta z = (\mathcal{H} \delta \eta - V_{\parallel} + \Psi)_o + \int_0^{\bar{r}_S} d\bar{r} n(\bar{r}) (V_{\parallel} - \Psi) - \int_0^{\bar{r}_S} d\bar{r} h(\bar{r}) \bar{r} (2\Psi' - C'_{\parallel}), \quad (2.26)$$

$$\begin{aligned} K = & \frac{3}{2} C_{\parallel o} - V_{\parallel o} + n_{\alpha} \delta x_o^{\alpha} (h - g)(0) + \int_0^{\bar{r}_S} d\bar{r} g(\bar{r}) \hat{\nabla}^2 \left(\Psi - \frac{1}{2} C_{\parallel} \right) \\ & - 2 \int_0^{\bar{r}_S} d\bar{r} h(\bar{r}) C_{\parallel} + \int_0^{\bar{r}_S} d\bar{r} h(\bar{r}) \hat{\nabla}^{\alpha} C_{\parallel \alpha}. \end{aligned} \quad (2.27)$$

Summing them up, we can write the scalar mode contribution to equation (2.23) as

$$\begin{aligned} \Delta D_{\text{sc.}} = & (1 - q(0)) \Psi_o + [\mathcal{H}_o (1 - q(0)) + (h - g)(0)] \delta \eta_o + V_{\parallel o} q(0) + \int_0^{\bar{r}_S} d\bar{r} \left(1 - \frac{1}{\mathcal{H} \bar{r}} \right) n(\bar{r}) V_{\parallel} \\ & - \int_0^{\bar{r}_S} d\bar{r} g(\bar{r}) \hat{\nabla}^2 \Psi - 2 \int_0^{\bar{r}_S} d\bar{r} f(\bar{r}) \Psi' + \int_0^{\bar{r}_S} d\bar{r} \left[2(h - g)(\bar{r}) + \left(\frac{1}{\mathcal{H} \bar{r}} - 2 \right) n(\bar{r}) \right] \Psi, \end{aligned} \quad (2.28)$$

and the tensor mode contribution as

$$\begin{aligned} \Delta D_{\text{t.}} = & -\frac{3}{2} C_{\parallel o} + \int_0^{\bar{r}_S} d\bar{r} \left(h(\bar{r}) + g(\bar{r}) - \frac{n(\bar{r})}{2} \right) C_{\parallel} - \int_0^{\bar{r}_S} d\bar{r} h(\bar{r}) \hat{\nabla}^{\alpha} C_{\parallel \alpha} \\ & + \frac{1}{2} \int_0^{\bar{r}_S} d\bar{r} g(\bar{r}) \hat{\nabla}^2 C_{\parallel} + \int_0^{\bar{r}_S} d\bar{r} f(\bar{r}) C'_{\parallel}. \end{aligned} \quad (2.29)$$

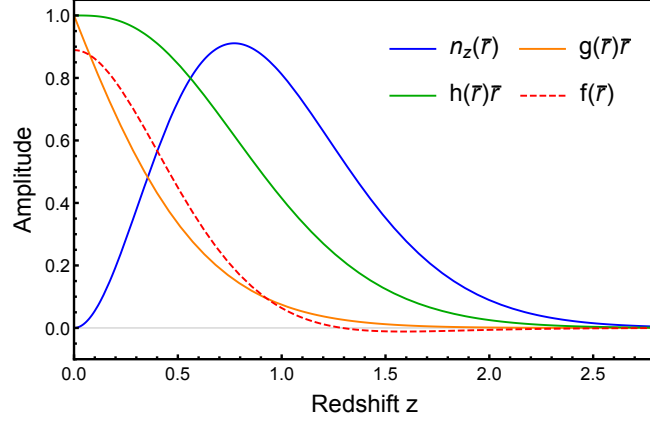


Figure 1: Redshift distribution function $n_z(\bar{r})$ of a Euclid-like survey, along with the kernels $h(\bar{r})\bar{r}$, $g(\bar{r})\bar{r}$ and $f(\bar{r})$, as a function of redshift z related to the comoving distance as stated in equation (2.3). The dashed line indicates that the value of $f(\bar{r})$ is negative.

The analytical expressions for the weak lensing angular power spectra given in sections 4 and 5 are valid for a general $n(\bar{r})$. For the numerical results presented in section 6, we specify a Euclid-like number density function,

$$n_z(z) = \frac{3}{2z_*} \left(\frac{z}{z_*} \right)^2 \exp(-(z/z_*)^{3/2}), \quad n(\bar{r}) = n_z(\bar{r}) \frac{dz}{d\bar{r}}, \quad (2.30)$$

where z_* is related to the median z_m as $z_* = z_m/1.412$, and we assume $z_m = 0.9$ as in [4]. Note that the dimensionless function $n_z(\bar{r})$ specifies the number of galaxies per redshift interval $dN/N_{tot} = n_z(\bar{r})dz$, implying the stated relation to the number density per radial interval $n(\bar{r})$. In figure 1, we plot the function $n_z(\bar{r})$ along with the resulting kernels $h(\bar{r})$, $g(\bar{r})$ and $f(\bar{r})$, where we have multiplied $h(\bar{r})$ and $g(\bar{r})$ with a factor \bar{r} to make these functions dimensionless. The redshift distribution $n_z(\bar{r})$ peaks at a value $z_p = 1.21141z_* \approx 0.77$, and approaches zero at $z \approx 3$, which sets the corresponding value for the depth of the survey \bar{r}_S . As $h(\bar{r})\bar{r}$ is simply defined as the integral of the normalized distribution function n from \bar{r} to \bar{r}_S , it is equal to 1 at $\bar{r} = 0$. While staying close to this value for low z , it then declines fast when approaching z_p . Similarly, $g(\bar{r})\bar{r}$ and $f(\bar{r})$ also decline fast with increasing z , pointing out that most of the contribution to the weak lensing observables from the line-of-sight integrals arise from redshifts below z_p .

Note that if all sources are located at a unique redshift z_s , hence $n(\bar{r}) = \delta(z(\bar{r}) - z_s) dz/d\bar{r}$ and $\bar{r}_S = \bar{r}(z_s) = \bar{r}_s$, we have

$$g(\bar{r}) = \frac{\bar{r}_s - \bar{r}}{\bar{r}_s \bar{r}}, \quad h(\bar{r}) = \frac{1}{\bar{r}}, \quad q(\bar{r}) = \frac{1}{\mathcal{H}_s \bar{r}_s}, \quad f(\bar{r}) = 1 - \frac{1}{\mathcal{H}_s \bar{r}_s}, \quad (2.31)$$

if $\bar{r} \leq \bar{r}_s$. If $\bar{r} > \bar{r}_s$, all of the above functions vanish. These relations allow us to recover the expressions for δD and γ_i from the expressions for ΔD and Γ_i . Hence, we can treat a sharp redshift distribution simply as a special case of a general distribution $n(\bar{r})$. In the result section 6, we apply both a Euclid-like $n(\bar{r})$ and a unique source redshift $z_s = 2$ and use the notations for the integrated observables, such as ΔD , to refer to both these cases.

3 Perturbation variables and their power spectra

The effect of weak lensing on observed images is determined by the perturbations of the FLRW metric and the peculiar motion. To numerically compute the power spectra of weak lensing observables, we thus need precise knowledge of the power spectra of these perturbation variables. For our work, we apply the power spectrum $P_{m,o}(k)$, describing the matter inhomogeneities $\delta_o(\mathbf{k})$ at $a_o = 1$, produced by CLASS [25] for a flat Λ CDM universe. The power spectra of other scalar perturbations, more precisely the potential Ψ and the radial velocity V_{\parallel} , can be related to the matter power spectrum $P_{m,o}(k)$ by applying the relations between the scalar perturbations and their growth functions, as we describe in section 3.1.

Apart from the scalar mode perturbation, inflation is also believed to produce tensor perturbations in most inflationary theories. They are quantified by the initial tensor power spectrum $P_T(k) \sim k^{n_T-3}$, with the tensor spectral index n_T being close to 0, which is further modulated by the tensor transfer function $T(k, \eta)$ at late time as we review in section 3.2. The presented properties are well known to literature (see e.g. [26] for a review on gravitational waves from inflation).

3.1 Scalar modes

Given today's matter power spectrum $P_{m,o}(k)$, its past evolution in a Λ CDM universe can be described by a scale-independent growth function $D(a)$,

$$\delta(k, a) = D(a)\delta_o(k), \quad P_m(k, a) = D^2(a)P_{m,o}(k), \quad (3.1)$$

given by the ordinary hypergeometric function ${}_2F_1$ (see e.g. [27]),

$$D(a) = \frac{\tilde{D}(a)}{\tilde{D}(a_o = 1)}, \quad \tilde{D}(a) = a {}_2F_1\left[\frac{1}{3}, 1, \frac{11}{6}, -\frac{a^3}{\Omega_m}(1 - \Omega_m)\right], \quad (3.2)$$

where we assumed $w = -1$ for the dark energy equation of state and normalized the growth function to unity today. To compute the weak lensing angular power spectra, we need to know the relation of the power spectra of all relevant scalar perturbation variables to the matter power spectrum $P_{m,o}(k)$. Furthermore, we need to know the respective growth functions of these scalar perturbations. This is, in essence, achieved by applying the ADM equations (see e.g. [28, 29]) in the comoving gauge to obtain the curvature power spectrum $P_{\zeta}(k)$ and the growth function of the metric perturbations in that gauge, and then apply the transformation to the Newtonian gauge used in this work. We refer to [23] and [30] for the details, and only state the results here.

The time-independent curvature perturbation $\zeta(\mathbf{x}) \equiv \zeta(\mathbf{x}, \eta)$ is related to the density perturbation $\delta_o(\mathbf{x})$ today as

$$\zeta(\mathbf{x}) = C\Delta^{-1}\delta_o(\mathbf{x}), \quad C = -\mathcal{H}^2 f \Sigma D, \quad (3.3)$$

where C is a constant, and we defined

$$f \equiv \frac{d \ln D}{d \ln a}, \quad \Sigma \equiv 1 + \frac{3}{2} \frac{\Omega_m}{f}. \quad (3.4)$$

Hence, we find the following relation between curvature and the matter power spectra,

$$\langle \zeta(\mathbf{k}) \zeta^*(\mathbf{k}') \rangle = (2\pi)^3 \delta(\mathbf{k} - \mathbf{k}') P_{\zeta}(k) = (2\pi)^3 \delta(\mathbf{k} - \mathbf{k}') \frac{C^2}{k^4} P_{m,o}(k). \quad (3.5)$$

The scalar potential Ψ and line-of-sight velocity $V_{\parallel} = V_{\alpha} n^{\alpha}$ are related to the curvature perturbation ζ as

$$\Psi(\mathbf{x}, \eta) = D_{\Psi}(\eta) \zeta(\mathbf{x}), \quad V_{\parallel}(\mathbf{x}, \eta) = D_V(\eta) \partial_{\parallel} \zeta(\mathbf{x}), \quad (3.6)$$

where the solutions for $D_{\Psi}(\eta)$ and $D_V(\eta)$ are given by

$$D_V = \frac{1}{\mathcal{H}\Sigma}, \quad D_{\Psi} = \mathcal{H}D_V - 1 = -\frac{1}{2}(D'_V + 1). \quad (3.7)$$

Transforming $\zeta(\mathbf{x})$ into Fourier space, equation (3.6) reads

$$\Psi(\mathbf{k}, \eta) = D_{\Psi}(\eta) \zeta(\mathbf{k}), \quad V_{\parallel}(\mathbf{k}, \mathbf{n}, \eta) = iD_V(\eta) \mathbf{n} \cdot \mathbf{k} \zeta(\mathbf{k}). \quad (3.8)$$

Hence, we obtain

$$\langle \Psi(\mathbf{k}, \eta) \Psi^*(\mathbf{k}', \eta') \rangle = (2\pi)^3 \delta(\mathbf{k} - \mathbf{k}') D_{\Psi}(\eta) D_{\Psi}(\eta') P_{\zeta}(k), \quad (3.9)$$

$$\langle V_{\parallel}(\mathbf{k}, \mathbf{n}, \eta) V_{\parallel}^*(\mathbf{k}', \mathbf{n}', \eta') \rangle = (2\pi)^3 \delta(\mathbf{k} - \mathbf{k}') D_V(\eta) D_V(\eta') (\mathbf{n} \cdot \mathbf{k}) (\mathbf{n}' \cdot \mathbf{k}') P_{\zeta}(k), \quad (3.10)$$

$$\langle V_{\parallel}(\mathbf{k}, \mathbf{n}, \eta) \Psi^*(\mathbf{k}', \eta') \rangle = (2\pi)^3 \delta(\mathbf{k} - \mathbf{k}') D_V(\eta) D_{\Psi}(\eta') i (\mathbf{n} \cdot \mathbf{k}) P_{\zeta}(k), \quad (3.11)$$

which will be the essential relations to calculate the contribution of scalar modes to the power spectra of the weak lensing observables. Note that any time derivatives of Ψ simply translate into time derivatives of the growth function $D_{\Psi}(\eta)$.

3.2 Tensor modes

The tensor metric perturbation $C_{\alpha\beta}$ can be decomposed into two independent polarization states C_{+} and C_{\times} :

$$C_{\alpha\beta}(\mathbf{k}, \eta) = e_{\alpha\beta}^{+}(\hat{\mathbf{k}}) C_{+}(\mathbf{k}, \eta) + e_{\alpha\beta}^{\times}(\hat{\mathbf{k}}) C_{\times}(\mathbf{k}, \eta), \quad (3.12)$$

where the polarization tensors $e_{\alpha\beta}^s$, $s \in \{+, \times\}$, are transverse, traceless and normalized through $e_{\alpha\beta}^s e^{s'\alpha\beta} = 2\delta^{ss'}$. Taking a generic direction $\hat{\mathbf{k}} = (\sin \vartheta \cos \varphi, \sin \vartheta \sin \varphi, \cos \vartheta)$, we can construct the polarization tensors as

$$e_{\alpha\beta}^{+}(\hat{\mathbf{k}}) \equiv e_{\alpha}^1(\hat{\mathbf{k}}) e_{\beta}^1(\hat{\mathbf{k}}) - e_{\alpha}^2(\hat{\mathbf{k}}) e_{\beta}^2(\hat{\mathbf{k}}), \quad e_{\alpha\beta}^{\times}(\hat{\mathbf{k}}) \equiv e_{\alpha}^1(\hat{\mathbf{k}}) e_{\beta}^2(\hat{\mathbf{k}}) + e_{\alpha}^2(\hat{\mathbf{k}}) e_{\beta}^1(\hat{\mathbf{k}}), \quad (3.13)$$

where

$$e_1(\hat{\mathbf{k}}) \equiv (\cos \vartheta \cos \varphi, \cos \vartheta \sin \varphi, -\sin \vartheta), \quad e_2(\hat{\mathbf{k}}) \equiv (-\sin \varphi, \cos \varphi, 0). \quad (3.14)$$

Furthermore, we define $e_{\alpha\beta}^p(\hat{\mathbf{k}})$ and $C_p(\mathbf{k}, \eta)$, where $p = \pm 1$, as

$$e_{\alpha\beta}^p(\hat{\mathbf{k}}) \equiv e_{\alpha\beta}^{+}(\hat{\mathbf{k}}) \pm i e_{\alpha\beta}^{\times}(\hat{\mathbf{k}}), \quad C_p(\mathbf{k}, \eta) = \frac{1}{2} (C_{+}(\mathbf{k}, \eta) \mp i C_{\times}(\mathbf{k}, \eta)), \quad (3.15)$$

fulfilling the properties

$$\sum_p e_{\alpha\beta}^p(\hat{\mathbf{k}}) C_p(\mathbf{k}, \eta) = e_{\alpha\beta}^{+}(\hat{\mathbf{k}}) C_{+}(\mathbf{k}, \eta) + e_{\alpha\beta}^{\times}(\hat{\mathbf{k}}) C_{\times}(\mathbf{k}, \eta) = C_{\alpha\beta}(\mathbf{k}, \eta), \quad (3.16)$$

and

$$\langle C_p(\mathbf{k}, \eta_o) C_p(\mathbf{k}', \eta_o) \rangle = \frac{1}{2} \langle C_{+}(\mathbf{k}, \eta_o) C_{+}(\mathbf{k}', \eta_o) \rangle = \frac{1}{2} \langle C_{\times}(\mathbf{k}, \eta_o) C_{\times}(\mathbf{k}', \eta_o) \rangle. \quad (3.17)$$

The correlation functions of the $C_s(\eta, \mathbf{k})$, with $s \in \{+, \times\}$, are given by

$$\langle C_s(\eta_1, \mathbf{k}_1) C_s^*(\eta_2, \mathbf{k}_2) \rangle = (2\pi)^3 \delta(\mathbf{k}_1 - \mathbf{k}_2) \delta_{ss'} \frac{1}{16} P_T(k_1, \eta_1, \eta_2), \quad (3.18)$$

where $P_T(k, \eta_1, \eta_2)$ is the total tensor power spectrum.³ It is determined by the tensor transfer function $T(k, \eta)$ and by the primordial tensor power spectrum $P_T(k)$ produced by inflation,

$$P_T(k, \eta_1, \eta_2) = T(k, \eta_1) T(k, \eta_2) P_T(k). \quad (3.19)$$

The primordial tensor power spectrum is given by

$$P_T(k) = \frac{2\pi^2}{k^3} A_T \left(\frac{k}{k_0} \right)^{n_T}, \quad (3.20)$$

where n_T is the tensor spectral index and A_T is the tensor amplitude. Note that, while the scalar growth function $D(a)$ is normalized to unity today, the tensor growth function $T(k, \eta)$ is normalized at some initial time period right after inflation.

After inflation, in the absence of anisotropic stress sourcing gravitational modes, the tensor modes propagate freely, damped only by the expansion of the universe. In a matter-dominated universe, the transfer function $T(k, \eta)$ is given by

$$T(k, \eta) = 3 \frac{j_1(k\eta)}{k\eta}, \quad (3.21)$$

which is a good approximation in more recent epochs with vacuum energy leading to an accelerated expansion.

4 Angular power spectra with the Limber approximation

Weak lensing angular power spectra are most commonly computed by using the Limber approximation, as first done by Kaiser in [7]. Here, we first present the weak lensing angular power spectra by adopting the Limber approximation. Their all-sky analysis and the comparison between the numerical results obtained with these two methods are presented in section 5 and 6, respectively.

The Limber approximation is based on splitting the line of sight into thin shells of width Δr with a planar geometry. Then, only those modes which are nearly perpendicular to the line of sight contribute to the angular power spectrum. More precisely, we consider a generic observable $A(\mathbf{n})$, which is a projection of a homogeneous and isotropic random field $F(\mathbf{x}, \bar{r})$ with some weight function $Q(\bar{r})$,

$$A(\mathbf{n}) = \int_0^{\bar{r}_S} d\bar{r} Q(\bar{r}) F(\bar{r}\mathbf{n}; \bar{r}), \quad (4.1)$$

where we are using \bar{r} to denote both the radial coordinate and the corresponding conformal time coordinate $\bar{\eta} = \bar{\eta}_o - \bar{r}$. Given such an observable $A(\mathbf{n})$, the relation between the

³Note that the other common notation for the tensor mode perturbations is $h_{\alpha\beta}$, usually differing from $C_{\alpha\beta}$ by a factor of two, $h_{\alpha\beta} = 2C_{\alpha\beta}$. This explains the additional factor of 1/4 in equation (3.18) compared with [36].

angular power spectrum $C^A(l)$ and the spatial power spectrum $P_F(k)$ applying the Limber approximation is given by

$$C^A(l) = \int_0^{\bar{r}_S} d\bar{r} \frac{Q(\bar{r})^2}{\bar{r}^2} P_F\left(k = \frac{l}{\bar{r}}; \bar{r}\right) = \int_0^{\bar{r}_S} d\bar{r} \frac{Q(\bar{r})^2}{\bar{r}^2} T_F^2\left(k = \frac{l}{\bar{r}}; \bar{r}\right) P_F\left(k = \frac{l}{\bar{r}}\right), \quad (4.2)$$

where $P_F(k)$ is the power spectrum of F at some reference time, and T_F is the respective growth function, $P_F(k; \bar{r}) \equiv T_F(k, \bar{r})P_F(k)$. Note that $Q(\bar{r})$ can not be equal to a delta distribution $\delta(\bar{r} - \bar{r}_s)$, as its square is not well-defined. In fact, it cannot be equal to any sharply varying function, as in the derivation of equation (4.2) given in [7], the function $Q(\bar{r})$ is required to be slowly varying such that it can be assumed to be constant on a small shell of width Δr . Consequently, it cannot account for any terms evaluated at a unique redshift. In particular, this applies to all terms evaluated at the observer position, which are thus ignored throughout this section.

The Limber approximation can also be applied to compute the cross angular power spectrum $C^{A_1 A_2}(l)$ of two observables,

$$A_1(\mathbf{n}) = \int_0^{\bar{r}_S} d\bar{r} Q_1(\bar{r}) F_1(\bar{\mathbf{r}}\mathbf{n}; \bar{r}), \quad A_2(\mathbf{n}) = \int_0^{\bar{r}_S} d\bar{r} Q_2(\bar{r}) F_2(\bar{\mathbf{r}}\mathbf{n}; \bar{r}), \quad (4.3)$$

as all steps in the derivation given in [7] remain equally valid. In this case, the Limber approximation yields

$$C^{A_1 A_2}(l) = \int_0^{\bar{r}_S} d\bar{r} \frac{Q_1(\bar{r})Q_2(\bar{r})}{\bar{r}^2} T_{F_1}\left(k = \frac{l}{\bar{r}}; \bar{r}\right) T_{F_2}\left(k = \frac{l}{\bar{r}}; \bar{r}\right) P_{F_1 F_2}\left(k = \frac{l}{\bar{r}}\right), \quad (4.4)$$

where $P_{F_1 F_2}(k)$ is the cross-power spectrum at some reference time, and T_{F_1} and T_{F_2} are the growth functions of F_1 and F_2 , respectively.

In the following, we derive the expressions for the weak lensing angular power spectra using equation (4.2). This will provide a comparison to the all-sky results calculated in section 5, which will point out the limitations of the Limber approximation. Indeed, we will see that it is inadequate for the calculation of general relativistic effects on weak lensing angular power spectra. It does not correctly account for scalar modes at low l , and for tensor modes at any scales.

4.1 Angular power spectrum of the magnification

Here, we use the Limber approximation to calculate the general relativistic effects in the angular power spectrum of the lensing magnification, where we start from the expression (2.23) for the observable ΔD , assuming some general source distribution function $n(\bar{r})$. Using equation (3.6), we evaluate the contribution of a k -mode,

$$\begin{aligned} \Delta D_{\text{sc}}(\mathbf{k}, \mathbf{n}) &= \int_0^{\bar{r}_S} d\bar{r} \left(1 - \frac{1}{\mathcal{H}\bar{r}}\right) n(\bar{r}) i D_V(\eta) \mathbf{n} \cdot \mathbf{k} \zeta(k) + \int_0^{\bar{r}_S} d\bar{r} g(\bar{r}) \bar{r}^2 k_{\perp}^2 D_{\Psi}(\bar{r}) \zeta(k) \\ &+ \int_0^{\bar{r}_S} d\bar{r} \left[2(h - g)(\bar{r}) + \left(\frac{1}{\mathcal{H}\bar{r}} - 2\right) n(\bar{r})\right] D_{\Psi}(\bar{r}) \zeta(k) - 2 \int_0^{\bar{r}_S} d\bar{r} f(\bar{r}) D'_{\Psi}(\bar{r}) \zeta(k), \end{aligned} \quad (4.5)$$

where \mathbf{k}_{\perp} is the projection of \mathbf{k} onto the plane perpendicular to the line of sight \mathbf{n} . For the Limber approximation, only modes with $\mathbf{k} = \mathbf{k}_{\perp}$ are relevant. Hence, the contribution of the line-of-sight term is fully vanishing, as $\mathbf{n} \cdot \mathbf{k}_{\perp} = 0$. For the remaining terms, the

Limber approximation (4.2) straight-forwardly yields the contribution to the angular power spectrum,

$$C_{\text{sc.}}^{\Delta D}(l) = \int_0^{\bar{r}_s} \frac{d\bar{r}}{\bar{r}^2} \left[\left(g(\bar{r})(l^2 - 2) + 2h(\bar{r}) + \left(\frac{1}{\mathcal{H}\bar{r}} - 2 \right) n(\bar{r}) \right) D_\Psi(\bar{r}) - 2f(\bar{r})D'_\Psi(\bar{r}) \right]^2 P_\zeta(l/\bar{r}). \quad (4.6)$$

However, as discussed in section 6, the source line-of-sight velocities significantly contribute to the angular power spectra of Δz and Δr . In other words, they are an important relativistic correction to ΔD , causing a deviation from the standard convergence K . Thus, the fact that these terms are vanishing in the Limber approximation constitutes a major inaccuracy. Indeed, a close look at the derivation of equation (4.2) given in [7] shows that the underlying assumptions of the Limber approximation break down for the velocity contribution. The fact that the function $j_0(k_3\Delta r/2)$ is non-negligible only for modes that are nearly perpendicular to the line of sight, i.e. for modes with small k_3 where k_3 is the line of sight component of the wave vector, is used in the derivation. However, the scalar product $\mathbf{n} \cdot \mathbf{k}$ yields another factor k_3 . As the function $k_3 j_0(k_3\Delta r/2)$ does not decrease for increasing k_3 , the assumption that only modes perpendicular to the line-of-sight need to be considered is violated, leading to this drastic inaccuracy.

While the Limber approximation is typically used to compute the contribution of scalar modes only to the angular power spectrum of some observable, the random field $F(\mathbf{x}, \bar{r})$ in equation (4.1) can, in principle, also correspond to some tensor contribution. The respective calculations for the tensor mode contribution to the magnification angular power spectrum are given in appendix B, and yield the following result:

$$C_{\text{t.}}^{\Delta D}(l) = \frac{1}{16} \int_0^{\bar{r}_s} \frac{d\bar{r}}{\bar{r}^2} \left[\left(-\frac{l^2}{2}g(\bar{r}) + 2h(\bar{r}) - \frac{n(\bar{r})}{2} \right) T(l/\bar{r}, \bar{r}) + f(\bar{r})T'(l/\bar{r}, \bar{r}) \right]^2 P_T(l/\bar{r}). \quad (4.7)$$

Taking equation (2.31) into account, the results given in equations (4.6) and (4.7) for the scalar and tensor mode contributions to $C^{\Delta D}(l)$ can be readily applied to a sharp redshift distribution $n(\bar{r}) = \delta(z(\bar{r}) - z_s)dz/d\bar{r}$. The terms $\sim n(\bar{r})$ evaluated at the source position are an exemption since, as previously discussed, the Limber approximation cannot account for such terms. Hence, for a sharp redshift distribution, the source terms have to be omitted additionally to the observer terms. With these restrictions, the total magnification angular power spectrum is given by

$$\begin{aligned} C_{\text{sc.}}^{\delta D}(l) &= \int_0^{\bar{r}_s} \frac{d\bar{r}}{\bar{r}^2} \left[\left(\frac{l^2(\bar{r}_s - \bar{r}) + 2\bar{r}}{\bar{r}_s \bar{r}} \right) D_\Psi(\bar{r}) + 2 \left(\frac{1 - \mathcal{H}_s \bar{r}_s}{\mathcal{H}_s \bar{r}_s} \right) D'_\Psi(\bar{r}) \right]^2 P_\zeta(l/\bar{r}), \\ C_{\text{t.}}^{\delta D}(l) &= \frac{1}{16} \int_0^{\bar{r}_s} \frac{d\bar{r}}{\bar{r}^2} \left[\left(\frac{l^2(\bar{r} - \bar{r}_s) + 2\bar{r}_s}{2\bar{r}_s \bar{r}} \right) T(l/\bar{r}, \bar{r}) + \left(\frac{\mathcal{H}_s \bar{r}_s - 1}{\mathcal{H}_s \bar{r}_s} \right) T'(l/\bar{r}, \bar{r}) \right]^2 P_T(l/\bar{r}). \end{aligned} \quad (4.8)$$

4.2 E- and B-mode angular power spectra

Starting from the expression for Γ_i given in equation (2.21), we can use the Limber approximation to calculate the angular power spectra $C^{\Gamma_i \Gamma_j}(\mathbf{l})$,

$$\langle \Gamma_i(\mathbf{l}) \Gamma_j^*(\mathbf{l}') \rangle = (2\pi)^2 \delta(\mathbf{l} - \mathbf{l}') C^{\Gamma_i \Gamma_j}(\mathbf{l}), \quad (4.9)$$

where $i, j \in \{1, 2\}$ and $C^{\Gamma_i \Gamma_j}(\mathbf{l}) = C^{\Gamma_i}(\mathbf{l})$. However, the definition of the shear components Γ_1 and Γ_2 depends on the choice of an orthonormal 2D-coordinate system on the sky, which can be rotated and is hence not uniquely defined. As a consequence, the angular power spectra $C^{\Gamma_i \Gamma_j}(\mathbf{l})$ depend not only on the absolute value l , but also on the angle φ between \mathbf{l} and the x -axis. However, if we decompose the shear signal into E- and B-modes [31],

$$\Gamma_1(\mathbf{l}) \pm i\Gamma_2(\mathbf{l}) = (E(\mathbf{l}) \pm iB(\mathbf{l})) e^{\pm i2\varphi}, \quad (4.10)$$

the resulting angular power spectra,

$$\langle X(\mathbf{l})Y^*(\mathbf{l}') \rangle = (2\pi)^2 \delta(\mathbf{l} - \mathbf{l}') C^{XY}(l), \quad (4.11)$$

where $X, Y \in \{E, B\}$ and $C^{XX}(l) \equiv C^X(l)$, depend only on the absolute value l . In this paper, when we refer to the shear components γ_1 and γ_2 defined for a unique source redshift, we indicate this by using the symbols \mathcal{E} and \mathcal{B} to denote E- and B-modes,

$$\gamma_1(\mathbf{l}) \pm i\gamma_2(\mathbf{l}) = (\mathcal{E}(\mathbf{l}) \pm i\mathcal{B}(\mathbf{l})) e^{\pm i2\varphi}. \quad (4.12)$$

To obtain expressions for the E- and B-mode power spectra, note that equation (4.10) can be rewritten into

$$\begin{pmatrix} E(\mathbf{l}) \\ B(\mathbf{l}) \end{pmatrix} = \begin{pmatrix} \cos(2\varphi) & \sin(2\varphi) \\ -\sin(2\varphi) & \cos(2\varphi) \end{pmatrix} \begin{pmatrix} \Gamma_1(\mathbf{l}) \\ \Gamma_2(\mathbf{l}) \end{pmatrix}, \quad (4.13)$$

which further yields the following relations between the angular power spectra of E- and B-modes and those of the shear components:

$$\begin{aligned} C^E(l) &= \cos^2(2\varphi) C^{\Gamma_1}(\mathbf{l}) + 2 \cos(2\varphi) \sin(2\varphi) C^{\Gamma_1 \Gamma_2}(\mathbf{l}) + \sin^2(2\varphi) C^{\Gamma_2}(\mathbf{l}), \\ C^{EB}(l) &= -\sin(2\varphi) \cos(2\varphi) C^{\Gamma_1}(\mathbf{l}) + \cos(4\varphi) C^{\Gamma_1 \Gamma_2}(\mathbf{l}) + \cos(2\varphi) \sin(2\varphi) C^{\Gamma_2}(\mathbf{l}), \\ C^B(l) &= \sin^2(2\varphi) C^{\Gamma_1}(\mathbf{l}) - 2 \cos(2\varphi) \sin(2\varphi) C^{\Gamma_1 \Gamma_2}(\mathbf{l}) + \cos^2(2\varphi) C^{\Gamma_2}(\mathbf{l}). \end{aligned} \quad (4.14)$$

To obtain the E- and B-mode angular power spectra, we start by applying the Limber approximation (4.4) to evaluate $C^{\Gamma_i \Gamma_j}(l, \varphi)$, $i, j \in \{1, 2\}$. First, consider the contribution of the scalar modes to the shear components given in equation (2.21), with the Fourier transform

$$\Gamma_{i\text{sc.}}(\mathbf{k}) = -\Phi_i^{\alpha\beta} \int_0^{\bar{r}_S} d\bar{r} g(\bar{r}) \bar{r}^2 k_{\perp}^{\alpha} k_{\perp}^{\beta} \Psi(\mathbf{k}, \bar{r}). \quad (4.15)$$

Applying equation (B.7), we obtain

$$\Gamma_{i\text{sc.}}(\mathbf{k}) = -\mathcal{A}_i(2\varphi) \int_0^{\bar{r}_S} d\bar{r} g(\bar{r}) \bar{r}^2 k_{\perp}^2 \Psi(\mathbf{k}, \bar{r}), \quad (4.16)$$

where $\mathcal{A}_i(\varphi)$ is defined in equation (B.8). Using the Limber approximation (4.4), this yields

$$C_{\text{sc.}}^{\Gamma_i \Gamma_j}(\mathbf{l}) = l^4 \mathcal{A}_i(2\varphi) \mathcal{A}_j(2\varphi) \int_0^{\bar{r}_S} d\bar{r} \frac{g(\bar{r})^2}{\bar{r}^2} D_{\Psi}^2(\bar{r}) P_{\zeta}(l/\bar{r}), \quad (4.17)$$

which, combined with equation (4.14), further yields

$$C_{\text{sc.}}^E(l) = l^4 \int_0^{\bar{r}_S} d\bar{r} \frac{g(\bar{r})^2}{\bar{r}^2} D_{\Psi}^2(\bar{r}) P_{\zeta}(l/\bar{r}), \quad C_{\text{sc.}}^B(l) = 0, \quad C_{\text{sc.}}^{EB}(l) = 0. \quad (4.18)$$

Hence, the dependence on the angle φ indeed vanishes, and the scalar modes contribute to the E-mode angular power spectrum only. For completeness, we also state the expressions for the tensor mode contributions to the E- and B-mode angular power spectra,

$$\begin{aligned} C_{\text{t.}}^E(l) &= \frac{1}{16} \int_0^{\bar{r}_s} \frac{d\bar{r}}{\bar{r}^2} \left[\left(1 - \frac{l^2}{2} \right) g(\bar{r}) - h(\bar{r}) + \frac{n(\bar{r})}{2} \right]^2 T(l/\bar{r}, \bar{r})^2 P_T(l/\bar{r}), \\ C^B(l) = C_{\text{t.}}^B(l) &= \frac{1}{16} l^2 \int_0^{\bar{r}_s} \frac{d\bar{r}}{\bar{r}^2} [h(\bar{r}) - 2g(\bar{r})]^2 T(l/\bar{r}, \bar{r})^2 P_T(l/\bar{r}), \end{aligned} \quad (4.19)$$

which can be derived using equations (B.3)–(B.7). The cross power spectrum between E- and B-modes is fully vanishing also for tensor modes, $C^{EB}(l)$, as implied by the opposite behavior of E- and B-modes under parity transformation.

Applying these results to a sharp redshift source distribution $n(\bar{r}) = \delta(z(\bar{r}) - z_s) dz/d\bar{r}$, where we omit terms evaluated at the now unique source redshift, we obtain

$$\begin{aligned} C_{\text{sc.}}^{\mathcal{E}}(l) &= l^4 \int_0^{\bar{r}_s} \frac{d\bar{r}}{\bar{r}^2} \left(\frac{\bar{r}_s - \bar{r}}{\bar{r}_s \bar{r}} \right)^2 D_{\Psi}^2(\bar{r}) P_{\zeta}(l/\bar{r}), \\ C_{\text{t.}}^{\mathcal{E}}(l) &= \frac{1}{16} \int_0^{\bar{r}_s} \frac{d\bar{r}}{\bar{r}^2} \left(\frac{l^2(\bar{r} - \bar{r}_s) - 2\bar{r}}{2\bar{r}_s \bar{r}} \right)^2 T(l/\bar{r}, \bar{r})^2 P_T(l/\bar{r}), \end{aligned} \quad (4.20)$$

for the scalar and tensor mode contributions to $C^{\mathcal{E}}(l)$, and

$$C^{\mathcal{B}}(l) = C_{\text{t.}}^{\mathcal{B}}(l) = \frac{1}{16} l^2 \int_0^{\bar{r}_s} \frac{d\bar{r}}{\bar{r}^2} \left(\frac{2\bar{r} - \bar{r}_s}{\bar{r}_s \bar{r}} \right)^2 T(l/\bar{r}, \bar{r})^2 P_T(l/\bar{r}), \quad (4.21)$$

for the tensor mode contribution to $C^{\mathcal{B}}(l)$.

4.3 Cross power spectrum of E-modes and δD

Here, we evaluate the cross angular power spectrum $C^{\Delta DE}(l)$ of E-modes and the magnification, again omitting all observer terms. Applying equation (4.5) for $\Delta D_{\text{sc.}}(\mathbf{k}, \mathbf{n})$ and equation (4.16) for $\Gamma_{i\text{sc.}}(\mathbf{k})$, the Limber approximation (4.4) yields

$$\begin{aligned} C_{\text{sc.}}^{\Delta D\Gamma_i}(\mathbf{l}) &= - \int_0^{\bar{r}_s} \frac{d\bar{r}}{\bar{r}^2} \left[\left(g(\bar{r})(l^2 - 2) + 2h(\bar{r}) + \left(\frac{1}{\mathcal{H}\bar{r}} - 2 \right) n(\bar{r}) \right) D_{\Psi}(\bar{r}) - 2f(\bar{r})D'_{\Psi}(\bar{r}) \right] \\ &\quad \times \mathcal{A}_i(2\varphi) l^2 g(\bar{r}) D_{\Psi}(\bar{r}) P_{\zeta}(l/\bar{r}), \end{aligned} \quad (4.22)$$

for the scalar mode contribution to $C^{\Delta D\Gamma_i}(\mathbf{l})$. Now, noting that equation (4.13) yields

$$\begin{aligned} C^{\Delta DE}(l) &= \cos(2\varphi) C^{\Delta D\Gamma_1}(\mathbf{l}) + \sin(2\varphi) C^{\Delta D\Gamma_2}(\mathbf{l}), \\ C^{\Delta DB}(l) &= -\sin(2\varphi) C^{\Delta D\Gamma_1}(\mathbf{l}) + \cos(2\varphi) C^{\Delta D\Gamma_2}(\mathbf{l}), \end{aligned} \quad (4.23)$$

we obtain

$$\begin{aligned} C_{\text{sc.}}^{\Delta DE}(\mathbf{l}) &= - \int_0^{\bar{r}_s} \frac{d\bar{r}}{\bar{r}^2} \left[\left(g(\bar{r})(l^2 - 2) + 2h(\bar{r}) + \left(\frac{1}{\mathcal{H}\bar{r}} - 2 \right) n(\bar{r}) \right) D_{\Psi}(\bar{r}) - 2f(\bar{r})D'_{\Psi}(\bar{r}) \right] \\ &\quad \times l^2 g(\bar{r}) D_{\Psi}(\bar{r}) P_{\zeta}(l/\bar{r}), \end{aligned} \quad (4.24)$$

and $C_{\text{sc.}}^{\Delta DB}(\mathbf{l}) = 0$, as expected from the different behaviour under parity transformation. Similarly, the tensor mode contribution to $C^{\Delta DB}(\mathbf{l})$ is also vanishing, while their contribution to $C^{\Delta DE}(\mathbf{l})$ is given by

$$C_{\text{t.}}^{\Delta DE}(\mathbf{l}) = \frac{1}{16} \int_0^{\bar{r}_s} \frac{d\bar{r}}{\bar{r}^2} \left[\left(-\frac{l^2 g(\bar{r})}{2} + 2h(\bar{r}) - \frac{n(\bar{r})}{2} \right) T(l/\bar{r}, \bar{r}) + f(\bar{r}) T'(l/\bar{r}, \bar{r}) \right] \\ \times \left[g(\bar{r}) \left(\frac{l^2 - 2}{2} \right) - \frac{n(\bar{r})}{2} + h(\bar{r}) \right] T(l/\bar{r}, \bar{r}) P_T(l/\bar{r}). \quad (4.25)$$

Applying these results to a sharp redshift distribution, $n(\bar{r}) = \delta(z(\bar{r}) - z_s) dz/d\bar{r}$, where we omit the terms evaluated at a now unique source redshift, we obtain

$$C_{\text{sc.}}^{\delta DE}(l) = \int_0^{\bar{r}_s} \frac{d\bar{r}}{\bar{r}^2} \left[\left(\frac{l^2(\bar{r}_s - \bar{r}) + 2\bar{r}}{\bar{r}_s \bar{r}} \right) D_\Psi(\bar{r}) + 2 \left(\frac{1 - \mathcal{H}_s \bar{r}_s}{\mathcal{H}_s \bar{r}_s} \right) D'_\Psi(\bar{r}) \right] \\ \times \left(\frac{\bar{r}_s - \bar{r}}{\bar{r}_s \bar{r}} \right) l^2 D_\Psi(\bar{r}) P_\zeta(l/\bar{r}), \quad (4.26)$$

and

$$C_{\text{t.}}^{\delta DE}(l) = \frac{1}{16} \int_0^{\bar{r}_s} \frac{d\bar{r}}{\bar{r}^2} \left[\left(\frac{l^2(\bar{r} - \bar{r}_s) + 2\bar{r}_s}{2\bar{r}_s \bar{r}} \right) T(l/\bar{r}, \bar{r}) + \left(\frac{\mathcal{H}_s \bar{r}_s - 1}{\mathcal{H}_s \bar{r}_s} \right) T'(l/\bar{r}, \bar{r}) \right] \\ \times \left(\frac{l^2(\bar{r} - \bar{r}_s) - 2\bar{r}}{2\bar{r}_s \bar{r}} \right) T(l/\bar{r}, \bar{r}) P_T(l/\bar{r}). \quad (4.27)$$

Note that $C^{\Delta DE}(l)$ (or $C^{\delta DE}(l)$) is different from $C^E(l) = C^{EE}(l)$ (or $C^\mathcal{E}(l) = C^{\mathcal{E}\mathcal{E}}(l)$). A two-dimensional deflection angle and the resulting distortion matrix are fully described by two degrees of freedom, namely the E- and B-modes. Thus, we would expect $C^{\Delta D}(l) = C^{\Delta DE}(l) = C^E(l)$ (or $C^{\delta DE}(l) = C^\mathcal{E}(l)$). However, as described in [13], the correct gauge-invariant description reveals that more physical information is needed to characterize all lensing observables, such as the source position and its rest frame. Consequently, the simple relation does not hold in reality. However, when taking into account only the scalar terms of the standard lensing convergence, i.e. the terms proportional to l^2 in equation (4.24) for $C_{\text{sc.}}^{\Delta DE}(l)$ (or equation (4.26) for $C_{\text{sc.}}^{\delta DE}(l)$), we recover the standard relation $C_{\text{sc.}}^K(l) = C_{\text{sc.}}^E(l) = -C_{\text{sc.}}^{KE}(l)$ (or $C_{\text{sc.}}^\kappa(l) = C_{\text{sc.}}^\mathcal{E}(l) = -C_{\text{sc.}}^{\kappa\mathcal{E}}(l)$). Note that the standard lensing convergence contributes to the distortion in the angular diameter distance with a negative sign.

5 All-sky analysis of the weak lensing angular power spectra

As discussed in the last section, the applicability of the Limber approximation is fairly limited, and, as we will see in the next section, it induces substantial errors on large scales. Indeed, none of the approximations commonly used in literature, such as the Limber or flat sky approximation, accurately describe the weak lensing angular power spectra on large scales (see e.g. [8]), where general relativistic effects become important.⁴ Nevertheless, this formalism has been sufficient for previous weak lensing surveys, where the relevant scales were not accessible due to the limited survey area. However, upcoming experiments will cover large fractions of the sky and will significantly surpass their predecessors in accuracy

⁴Note that what we refer to as the Limber approximation corresponds to a combined flat sky, Limber and integral variable approximation as described in [8].

and survey depth. Hence, an accurate study of large scales is crucial to correctly interpret the vast amount of data accessible in the near future. In this section, we accurately evaluate the weak lensing angular power spectra based on (spin-weighted) spherical harmonics, and we will refer to this method as the *all-sky* approach, emphasizing that it does not use any approximation and is thus precise even on the largest scales.

Since we are now considering weak lensing signals on the whole sky, the 2D-Fourier decomposition assuming a planar geometry is clearly inadequate. Instead, a signal $A(\mathbf{n})$ observed on the whole sky can be decomposed using the spherical harmonics decomposition,

$$A(\mathbf{n}) = \sum a_{lm}^A Y_{lm}(\mathbf{n}), \quad a_{lm}^A = \int d\Omega A(\mathbf{n}) Y_{lm}^*(\mathbf{n}), \quad (5.1)$$

where we choose the convention

$$Y_{lm}(\theta, \phi) = \sqrt{\frac{(2l+1)(l-m)!}{4\pi(l+m)!}} P_l^m(\cos\theta) e^{im\phi}, \quad P_l^m(x) = (-1)^m (1-x^2)^{m/2} \frac{d^m}{dx^m} P_l(x), \quad (5.2)$$

for the spherical harmonics $Y_{lm}(\theta, \phi)$ and the associated Legendre polynomials $P_l^m(x)$. The angular power spectrum $C^A(l)$ is related to the spherical harmonics coefficients a_{lm}^A as

$$\langle a_{lm}^A (a_{l'm'}^A)^* \rangle = \delta_{ll'} \delta_{mm'} C^A(l). \quad (5.3)$$

In section 5.1, we use the spherical harmonics decomposition to calculate the magnification angular power spectrum. While the spherical harmonics decomposition is applicable for ΔD being a scalar (spin-0) quantity, this is not true for the shear signal depending on the choice of an arbitrary basis on the sky. We need a more general decomposition instead, the spin-weighted spherical harmonics decomposition, which we apply in section 5.2 to provide the accurate expressions for the E- and B-mode power spectra. Finally, section 5.3 contains the expression for the cross angular power spectrum between ΔD and the shear E-modes.

We base our calculations on the formalism described in appendix A of [14]. In particular, we will repeatedly apply the fundamental equation

$$\int d\Omega Y_{lm}^* (1-\mu^2)^{|r|/2} e^{ir\phi} e^{ix\mu} = \sqrt{4\pi(2l+1)} \sqrt{\frac{(l+|r|)!}{(l-|r|)!}} i^r i^l \frac{j_l(x)}{x^{|r|}} \delta_{mr}, \quad (5.4)$$

and work with the quantities $A(\mathbf{n}, \mathbf{k})$ and $a_{lm}^A(\mathbf{k})$ denoting the contribution of a single Fourier mode,

$$A(\mathbf{n}) \equiv \int \frac{d^3\mathbf{k}}{(2\pi)^3} A(\mathbf{k}, \mathbf{n}), \quad a_{lm}^A(\mathbf{k}) \equiv \int d\Omega A(\mathbf{k}, \mathbf{n}) Y_{lm}^*(\hat{\mathbf{n}}), \quad a_{lm}^A = \int \frac{d^3\mathbf{k}}{(2\pi)^3} a_{lm}^A(\mathbf{k}). \quad (5.5)$$

Throughout this section, the coordinate \bar{r} in expressions such as $\Psi(\mathbf{k}, \bar{r})$ or $C_{\alpha\beta}(\mathbf{k}, \bar{r})$ will be used to denote the conformal time coordinate $\eta(\bar{r}) = \eta_o - \bar{r}$.

5.1 All-sky angular power spectrum of the magnification

Let us start with the non-integrated expression δD , i.e. the magnification signal if all sources are located at a unique redshift z_s . To keep the expressions manageable, let us first look at

the scalar contribution $\delta D_{\text{sc.}}$ only. First, we compute the contribution from a single Fourier mode,

$$\begin{aligned} \delta D_{\text{sc.}}(\mathbf{k}, \mathbf{n}) = & \left(1 - \frac{1}{\bar{r}_s \mathcal{H}_s}\right) \Psi(\mathbf{k}, 0) + \left(\mathcal{H}_o - \frac{\mathcal{H}_o}{\bar{r}_s \mathcal{H}_s} + \frac{1}{\bar{r}_s}\right) \delta\eta(\mathbf{k}, 0) + \frac{V_{\parallel}(\mathbf{k}, \mathbf{n}, 0)}{\bar{r}_s \mathcal{H}_s} \\ & - \left(2 - \frac{1}{\mathcal{H}_s \bar{r}_s}\right) \Psi(\mathbf{k}, \bar{r}_s) e^{ix_s \mu} + \left(1 - \frac{1}{\mathcal{H}_s \bar{r}_s}\right) V_{\parallel}(\mathbf{k}, \mathbf{n}, \bar{r}_s) e^{ix_s \mu} + \frac{2}{\bar{r}_s} \int_0^{\bar{r}_s} d\bar{r} \Psi(\mathbf{k}, \bar{r}) e^{ix \mu} \\ & - \int_0^{\bar{r}_s} d\bar{r} \left(\frac{\bar{r}_s - \bar{r}}{\bar{r}_s \bar{r}}\right) \hat{\nabla}^2 (\Psi(\mathbf{k}, \bar{r}) e^{ix \mu}) - 2 \left(1 - \frac{1}{\mathcal{H}_s \bar{r}_s}\right) \int_0^{\bar{r}_s} d\bar{r} \Psi'(\mathbf{k}, \bar{r}) e^{ix \mu}, \end{aligned} \quad (5.6)$$

where we chose \mathbf{k} to be aligned with the z -axis, $\mathbf{k} = k\mathbf{e}_z$, and defined $x = k\bar{r}$ and $\mu = \cos\theta = \mathbf{n} \cdot \hat{\mathbf{k}}$. As a next step, we need to compute the spherical harmonic coefficients,

$$a_{lm \text{ sc.}}^{\delta D}(\mathbf{k}) = \int d\Omega \delta D_{\text{sc.}}(\mathbf{k}, \mathbf{n}) Y_{lm}^*(\mathbf{n}). \quad (5.7)$$

Equation (5.4) with $r = 0$ enables us to perform this calculations for all terms appearing in $\delta D_{\text{sc.}}$, except for the term $\propto V_{\parallel}(0, \mathbf{k}, \mathbf{n})$, for which we use the relation

$$\int d\Omega \mu Y_{lm}^* = 2\sqrt{\frac{\pi}{3}} \int d\Omega Y_{10} Y_{lm}^* = 2\sqrt{\frac{\pi}{3}} \delta_{l1} \delta_{m0}. \quad (5.8)$$

We obtain

$$a_{lm \text{ sc.}}^{\delta D}(\mathbf{k}) = i^l \sqrt{4\pi(2l+1)} \zeta(\mathbf{k}) \delta_{m0} \mathcal{S}_l^{\delta D}(k), \quad (5.9)$$

where

$$\begin{aligned} \mathcal{S}_l^{\delta D}(k) = & \left(1 - \frac{1}{\bar{r}_s \mathcal{H}_s}\right) D_{\Psi}(0) \delta_{l0} + \left(\mathcal{H}_o - \frac{\mathcal{H}_o}{\bar{r}_s \mathcal{H}_s} + \frac{1}{\bar{r}_s}\right) D_V(0) \delta_{l0} + \frac{1}{3} \frac{D_V(0)k}{\bar{r}_s \mathcal{H}_s} \delta_{l1} \\ & - \left(2 - \frac{1}{\mathcal{H}_s \bar{r}_s}\right) D_{\Psi}(\bar{r}_s) j_l(x_s) + \left(1 - \frac{1}{\mathcal{H}_s \bar{r}_s}\right) D_V(\bar{r}_s) k j_l'(x_s) + \frac{2}{\bar{r}_s} \int_0^{\bar{r}_s} d\bar{r} D_{\Psi}(\bar{r}) j_l(x) \\ & + l(l+1) \int_0^{\bar{r}_s} d\bar{r} \left(\frac{\bar{r}_s - \bar{r}}{\bar{r}_s \bar{r}}\right) D_{\Psi}(\bar{r}) j_l(x) - 2 \left(1 - \frac{1}{\mathcal{H}_s \bar{r}_s}\right) \int_0^{\bar{r}_s} d\bar{r} D'_{\Psi}(\bar{r}) j_l(x). \end{aligned} \quad (5.10)$$

Note that the factor δ_{m0} in equation (5.9) is a result of choosing \mathbf{k} to be aligned with the z -axis. Furthermore, note that the term $\propto j_l'(x_z)$ occurs since multiplications with $i\mu$ can be transformed into partial derivatives ∂_x . We also applied the relation

$$a_{lm} \left[\hat{\nabla}^2 A \right] = -l(l+1) a_{lm}^A, \quad (5.11)$$

which follows from partial integration and the following fundamental property of spherical harmonics, $\hat{\nabla}^2 Y_{lm} = -l(l+1) Y_{lm}$.

Finally, we compute the scalar contribution $C_{\text{sc.}}^{\delta D}(l)$ to the magnification angular power spectrum,

$$C_{\text{sc.}}^{\delta D}(l) = \left\langle a_{lm \text{ sc.}}^{\delta D} \left(a_{lm \text{ sc.}}^{\delta D} \right)^* \right\rangle = \int \int \frac{d^3 \mathbf{k}}{(2\pi)^3} \frac{d^3 \mathbf{k}'}{(2\pi)^3} \left\langle a_{lm \text{ sc.}}^{\delta D}(\mathbf{k}) \left(a_{lm \text{ sc.}}^{\delta D}(\mathbf{k}') \right)^* \right\rangle. \quad (5.12)$$

Hence, $C_{\text{sc.}}^{\delta D}(l)$ is given by an integral over all $\mathbf{k}, \mathbf{k}' \in \mathbb{R}^3$, while we have only computed $a_{lm\text{sc.}}^{\delta D}(\mathbf{k})$ for a wave vector aligned with the z -axis. However, as explained in appendix C, a summation over all m allows us to replace the general \mathbf{k} with $k\mathbf{e}_z$, which leads to the result

$$C_{\text{sc.}}^{\delta D}(l) = \frac{2}{\pi} \int dk k^2 P_\zeta(k) (\mathcal{S}_l^{\delta D}(k))^2. \quad (5.13)$$

As we have not assumed any approximation to derive this expression, it is valid on all scales at the linear order. The contribution of the standard lensing convergence is proportional to the factor $l(l+1)$, vanishing at $l=0$, as this contribution is just the re-shuffling of the fluctuation and averages to zero over the sky. The other terms in this expressions arise from the distortion in radial coordinate and redshift and an additional gravitational potential term evaluated at the source, as described in section 2.2. In particular, all contributions that cannot be treated within the Limber approximation, i.e. velocity terms and terms evaluated at the observer position or a unique source redshift, are now fully included. Note that in the Limber approximation, the term in equation (4.8) arising from the convergence has a pre-factor l^2 , which is practically equal to $l(l+1)$ for large l . Indeed, as we will see in section 6, the Limber approximation is fairly accurate on almost all scales, and the all-sky approach provides significant corrections only for the lowest l .

Similarly, the tensor contribution to $C^{\delta D}(l)$ can be calculated. First, note that

$$\int_0^{\bar{r}_s} \frac{d\bar{r}}{\bar{r}} \hat{\nabla}_\alpha C_\parallel^\alpha = - \int_0^{\bar{r}_s} \frac{d\bar{r}}{\bar{r}} C_\parallel - \int_0^{\bar{r}_s} d\bar{r} C'_\parallel - C_\parallel + C_{\parallel o}, \quad (5.14)$$

where we used equations (A.3) and (A.6), along with the fact that $C_{\alpha\beta}$ is divergence-less and that the partial derivative $\partial/\partial\bar{r}$ relates to the total derivative $d/d\bar{r} = -d/d\eta$ as $d/d\bar{r} = \partial/\partial\bar{r} - \partial/\partial\eta$. Hence, we can rewrite the tensor mode δD_t into the more practical form

$$\begin{aligned} \delta D_t = & -\frac{5}{2}C_{\parallel o} + \frac{1}{2}C_\parallel + \int_0^{\bar{r}_s} d\bar{r} \left(\frac{3\bar{r}_s - \bar{r}}{\bar{r}_s \bar{r}} \right) C_\parallel + \int_0^{\bar{r}_s} d\bar{r} \left(\frac{\bar{r}_s - \bar{r}}{2\bar{r}_s \bar{r}} \right) \hat{\nabla}^2 C_\parallel \\ & + \left(2 - \frac{1}{\mathcal{H}_s \bar{r}_s} \right) \int_0^{\bar{r}_s} d\bar{r} C'_\parallel. \end{aligned} \quad (5.15)$$

Using equation (D.6), we calculate that the contribution of a single Fourier mode aligned with the z -axis, $\mathbf{k} = k\mathbf{e}_z$, is given by

$$\begin{aligned} \delta D_t(\mathbf{k}, \mathbf{n}, p) = & C_p(\mathbf{k}) e^{ip2\phi} \left[-\frac{5}{2}(1-\mu^2)T(\mathbf{k}, 0) + \frac{1}{2}(1-\mu^2)T(\mathbf{k}, \bar{r}_s) e^{ix_s\mu} \right. \\ & + \int_0^{\bar{r}_s} d\bar{r} \left(\frac{3\bar{r}_s - \bar{r}}{\bar{r}_s \bar{r}} \right) (1-\mu^2)T(\mathbf{k}, \bar{r}) e^{ix\mu} + \int_0^{\bar{r}_s} d\bar{r} \left(\frac{\bar{r}_s - \bar{r}}{2\bar{r}_s \bar{r}} \right) \hat{\nabla}^2 ((1-\mu^2)T(\mathbf{k}, \bar{r}) e^{ix\mu}) \\ & \left. + \left(2 - \frac{1}{\mathcal{H}_s \bar{r}_s} \right) \int_0^{\bar{r}_s} d\bar{r} (1-\mu^2)T'(\mathbf{k}, \bar{r}) e^{ix\mu} \right], \end{aligned} \quad (5.16)$$

where we have split $\delta D_t(\mathbf{k}, \hat{\mathbf{n}})$ into the contributions from C_p , $p = \pm 1$ following equation (3.16). Now, we can compute the spherical harmonic coefficients by applying equation (5.4) for the cases $r = \pm 1$. We obtain

$$a_{lm\text{t.}}^{\delta D}(\mathbf{k}) = -i^l \sqrt{4\pi(2l+1)} \sqrt{\frac{(l+2)!}{(l-2)!}} \sum_{p=\pm 1} C_p(\mathbf{k}) \delta_{m2}^p \mathcal{T}_l^{\delta D}(k), \quad (5.17)$$

where we defined

$$\begin{aligned} \mathcal{T}_l^{\delta D}(k) = & -\frac{1}{6}T(k, 0)\delta_{l2} + \frac{1}{2}T(k, \bar{r}_s)\frac{j_l(x_s)}{x_s^2} + \int_0^{\bar{r}_s} d\bar{r} \left(\frac{3\bar{r}_s - \bar{r}}{\bar{r}_s \bar{r}} \right) T(k, \bar{r}) \frac{j_l(x)}{x^2} \\ & - l(l+1) \int_0^{\bar{r}_s} d\bar{r} \left(\frac{\bar{r}_s - \bar{r}}{2\bar{r}_s \bar{r}} \right) T(k, \bar{r}) \frac{j_l(x)}{x^2} + \left(2 - \frac{1}{\mathcal{H}_s \bar{r}_s} \right) \int_0^{\bar{r}_s} d\bar{r} T'(k, \bar{r}) \frac{j_l(x)}{x^2}, \end{aligned} \quad (5.18)$$

and introduced the symbol δ_{m2}^p being equal to 1 when $m = 2p$, and 0 otherwise. Note that this factor δ_{m2}^p implies that the contribution is zero for $l = 0, 1$. Furthermore, we used that

$$\lim_{x \rightarrow 0} \frac{j_l(x)}{x^2} = \begin{cases} \frac{1}{15} & \text{for } l = 2, \\ 0 & \text{for } l > 2. \end{cases} \quad (5.19)$$

Finally, we obtain for the tensor contribution to $C^{\delta D}(l)$:

$$\begin{aligned} C_{\text{t}}^{\delta D}(l) = & \frac{1}{2l+1} \sum_{m=-l}^l \int \int \frac{d^3 \mathbf{k}}{(2\pi)^3} \frac{d^3 \mathbf{k}'}{(2\pi)^3} \left\langle a_{lm\text{t}}^{\delta D}(\mathbf{k}) (a_{lm\text{t}}^{\delta D}(\mathbf{k}'))^* \right\rangle \\ = & \frac{1}{8\pi} \frac{(l+2)!}{(l-2)!} \delta_{l \geq 2} \int dk k^2 P_T(k) (\mathcal{T}_l^{\delta D}(k))^2, \end{aligned} \quad (5.20)$$

where again, we replaced the general \mathbf{k} with a k -vector aligned with the line-of-sight, as explained in appendix C.

As for the scalar modes, the term proportional to $l(l+1)$ corresponds to the contribution from the standard lensing convergence, and other terms arise from the distortion in the radial coordinate and in redshift and from an additional term evaluated at the source position as described in section 2.2. While for scalar modes, the angular power spectrum computed from the Limber approximation quickly approaches the one from the all-sky approach with increasing l , this is not the case for tensor modes, where there is a substantial difference between these two methods on all scales, as we will show and further discuss in section 6.

Having obtained the results for the scalar and tensor contributions to $C^{\delta D}(l)$, the magnification angular power spectrum with all sources located at a unique redshift z_s , we now want to apply an arbitrary distribution function $n(\bar{r})$ instead of a sharp redshift distribution to evaluate $C^{\Delta D}(l)$. For that, we start with the integrated expression given in equation (2.23) for ΔD instead of equation (2.10) for δD . This only affects the functions of \bar{r} appearing in the expressions, and does not have any other implications on the calculations. Hence, the result for $C^{\delta D}(l)$ can be easily rewritten into a more general expression for $C^{\Delta D}(l)$ by replacing the operators $\mathcal{S}_l^{\delta D}(k)$ and $\mathcal{T}_l^{\delta D}(k)$ with

$$\begin{aligned} \mathcal{S}_l^{\Delta D}(k) = & (1 - q(0))D_\Psi(0)\delta_{l0} + (\mathcal{H}_o - \mathcal{H}_o q(0) + (h - g)(0))D_V(0)\delta_{l0} + \frac{1}{3}q(0)D_V(0)k\delta_{l1} \\ & + \int_0^{\bar{r}_s} d\bar{r} \left[2(h - g)(\bar{r}) + \left(\frac{1}{\mathcal{H}\bar{r}} - 2 \right) n(\bar{r}) \right] D_\Psi(\bar{r})j_l(x) + l(l+1) \int_0^{\bar{r}_s} d\bar{r} g(\bar{r})D_\Psi(\bar{r})j_l(x) \\ & + \int_0^{\bar{r}_s} d\bar{r} \left(1 - \frac{1}{\mathcal{H}\bar{r}} \right) n(\bar{r})D_V(\bar{r})kj_l'(x) + 2 \int_0^{\bar{r}_s} d\bar{r} (q(\bar{r}) - h(\bar{r})\bar{r})D'_\Psi(\bar{r})j_l(x), \end{aligned} \quad (5.21)$$

and

$$\begin{aligned} \mathcal{T}_l^{\Delta D}(k) = & -\frac{1}{6}T(k, 0)\delta_{l2} + \int_0^{\bar{r}_s} d\bar{r} \left(\frac{n(\bar{r})}{2} + 2h(\bar{r}) + g(\bar{r}) \right) T(k, \bar{r}) \frac{j_l(x)}{x^2} \\ & - \frac{l(l+1)}{2} \int_0^{\bar{r}_s} d\bar{r} g(\bar{r})T(k, \bar{r}) \frac{j_l(x)}{x^2} + \int_0^{\bar{r}_s} d\bar{r} (2\bar{r}h(\bar{r}) - q(\bar{r}))T'(k, \bar{r}) \frac{j_l(x)}{x^2}. \end{aligned} \quad (5.22)$$

5.2 All-sky E- and B-mode angular power spectra

Unlike the magnification quantified by the distortion in the angular diameter distance δD , which is a scalar quantity, the shear components depend on the choice of an arbitrary basis (θ, ϕ) orthonormal to \mathbf{n} on the sky. For example, rotating the basis by 45° transforms γ_1 into γ_2 and vice versa. This behavior is mathematically better described by replacing the shear components γ_1 and γ_2 with the quantities $\pm_2\gamma \equiv \gamma_1 \pm i\gamma_2$. These are spin-2 quantities, i.e., rotating the coordinate system around \mathbf{n} by some angle α yields

$$\pm_2\gamma \mapsto e^{\pm 2i\alpha} \pm_2\gamma. \quad (5.23)$$

To decompose the shear signal on the sky, we have to replace the spherical harmonics $Y_{lm}(\mathbf{n})$ with the more general spin-weighted spherical harmonics,

$${}_sY_{lm} = \begin{cases} \sqrt{\frac{(l-s)!}{(l+s)!}} \bar{\eth}^s Y_{lm}, & 0 \leq s \leq l, \\ \sqrt{\frac{(l+s)!}{(l-s)!}} \eth^{-s} Y_{lm}, & 0 \leq -s \leq l, \\ 0, & l < |s|, \end{cases} \quad (5.24)$$

where \eth and $\bar{\eth}$ are spin-raising and, respectively, -lowering operators defined through

$$\eth_s f = -\sin^s \theta \left[\frac{\partial}{\partial \theta} + \frac{i}{\sin \theta} \frac{\partial}{\partial \phi} \right] \sin^{-s} \theta_s f, \quad \bar{\eth}_s f = -\sin^{-s} \theta \left[\frac{\partial}{\partial \theta} + \frac{i}{\sin \theta} \frac{\partial}{\partial \phi} \right] \sin^s \theta_s f. \quad (5.25)$$

The spin-2 quantities $\pm_2\gamma(\mathbf{n})$ are decomposed as

$$a_{lm}^{\gamma\pm} \equiv \int d\Omega \pm_2\gamma(\mathbf{n}) \pm_2 Y_{lm}^*(\mathbf{n}). \quad (5.26)$$

Applying the definitions of the spin-weighted spherical harmonics and partial integration, we obtain the alternative expressions

$$\begin{aligned} a_{lm}^{\gamma+}(\mathbf{k}) &= \delta_{l \geq 2} \sqrt{\frac{(l-2)!}{(l+2)!}} \int d\Omega \bar{\eth}^2 {}_2\gamma(\mathbf{k}, \mathbf{n}) Y_{lm}^*(\hat{\mathbf{n}}), \\ a_{lm}^{\gamma-}(\mathbf{k}) &= \delta_{l \geq 2} \sqrt{\frac{(l-2)!}{(l+2)!}} \int d\Omega \eth^2 {}_{-2}\gamma(\mathbf{k}, \mathbf{n}) Y_{lm}^*(\hat{\mathbf{n}}). \end{aligned} \quad (5.27)$$

Note that the definition of spin-weighted spherical harmonics implies that $a_{lm}^{\gamma\pm}$ is vanishing for $l = 0$ and $l = 1$, which we express with the symbol $\delta_{l \geq 2}$. Defining the spin-1 basis m_\pm^α as

$$m_\pm^\alpha \equiv \frac{1}{\sqrt{2}}(\theta^\alpha \mp i\phi^\alpha) = \frac{1}{\sqrt{2}} \begin{pmatrix} \cos \theta \cos \phi \pm i \sin \phi \\ \cos \theta \sin \phi \mp i \cos \phi \\ -\sin \theta \end{pmatrix}, \quad (5.28)$$

the spin-weighted spherical harmonics with spin-2 can be written as [14]

$$\pm_2 Y_{lm} = 2 \sqrt{\frac{(l-2)!}{(l+2)!}} m_\mp^i m_\mp^j \nabla_i \nabla_j Y_{lm}, \quad l \geq 2. \quad (5.29)$$

Furthermore, we define the shear matrix

$$\gamma_{\alpha\beta} \equiv {}_2\gamma m_+^\alpha m_+^\beta + {}_{-2}\gamma m_-^\alpha m_-^\beta, \quad (5.30)$$

which implies the relations

$$\begin{aligned} {}_{\pm 2}\gamma &= m_\mp^\alpha m_\mp^\beta \gamma_{\alpha\beta}, \quad \gamma_i = \frac{1}{2} \Phi_i^{\alpha\beta} \gamma_{\alpha\beta}, \\ \Phi_1^{\alpha\beta} &= m_+^\alpha m_+^\beta + m_-^\alpha m_-^\beta, \quad \Phi_2^{\alpha\beta} = i \left(m_+^\alpha m_+^\beta - m_-^\alpha m_-^\beta \right). \end{aligned} \quad (5.31)$$

From equation (2.17) for the shear components, we conclude that

$$\gamma_{\alpha\beta} = -C_{\alpha\beta o} - C_{\alpha\beta} + \int_0^{\bar{r}_s} d\bar{r} \left(\frac{\bar{r}_s - \bar{r}}{\bar{r}_s \bar{r}} \right) \hat{\nabla}_\alpha \hat{\nabla}_\beta (2\Psi - C_\parallel) + 2 \int_0^{\bar{r}_s} \frac{d\bar{r}}{\bar{r}} \hat{\nabla}_\beta C_{\parallel\alpha}. \quad (5.32)$$

Hence, we can write ${}_{\pm 2}\gamma$ as

$${}_{\pm 2}\gamma = {}_{\pm 2}S + {}_{\pm 2}T0 + {}_{\pm 2}T1 + {}_{\pm 2}T2 + {}_{\pm 2}T3, \quad (5.33)$$

where we have defined

$${}_{\pm 2}S \equiv m_\mp^\alpha m_\mp^\beta \int_0^{\bar{r}_s} d\bar{r} \frac{2(\bar{r}_s - \bar{r})}{\bar{r}_s \bar{r}} \hat{\nabla}_\alpha \hat{\nabla}_\beta \Psi, \quad (5.34)$$

and

$$\begin{aligned} {}_{\pm 2}T0 &\equiv -m_\mp^\alpha m_\mp^\beta C_{\alpha\beta o}, \quad {}_{\pm 2}T3 \equiv -m_\mp^\alpha m_\mp^\beta C_{\alpha\beta}, \quad {}_{\pm 2}T2 \equiv 2 m_\mp^\alpha m_\mp^\beta \int_0^{\bar{r}_s} \frac{d\bar{r}}{\bar{r}} \hat{\nabla}_\beta C_{\alpha\parallel}, \\ {}_{\pm 2}T1 &\equiv -m_\mp^\alpha m_\mp^\beta \int_0^{\bar{r}_s} d\bar{r} \left(\frac{\bar{r}_s - \bar{r}}{\bar{r}_s \bar{r}} \right) \hat{\nabla}_\alpha \hat{\nabla}_\beta C_\parallel. \end{aligned} \quad (5.35)$$

To calculate the angular power spectra $C^\mathcal{E}(l)$ and $C^\mathcal{B}(l)$, we proceed as follows: First, we compute the contributions of an individual Fourier mode ${}_{\pm 2}\gamma(\mathbf{k}, \mathbf{n})$ for a wave vector \mathbf{k} aligned with the z -axis, $\mathbf{k} = k\mathbf{e}_z$. Next, we apply the spin-raising and -lowering operators to obtain $\bar{\partial}^2 {}_{-2}\gamma(\mathbf{k}, \mathbf{n})$ and $\bar{\partial}^2 {}_2\gamma(\mathbf{k}, \mathbf{n})$, and compute $a_{lm}^{\gamma\pm}(\mathbf{k})$ from equation (5.27). Then, we split $a_{lm}^{\gamma\pm}(\mathbf{k})$ into $a_{lm}^\mathcal{E}(\mathbf{k})$ and $a_{lm}^\mathcal{B}(\mathbf{k})$, distinguishable by their parity transformation properties. Having obtained the equations for $a_{lm}^\mathcal{E}(\mathbf{k})$ and $a_{lm}^\mathcal{B}(\mathbf{k})$, we finally derive the expressions for the E- and B-mode angular power spectra.

5.2.1 Calculation of $a_{lm}^{\gamma\pm}(k)$

First, assuming that \mathbf{k} is aligned with the z -axis, we calculate ${}_{\pm 2}\gamma(\mathbf{k}, \mathbf{n})$ defined as

$${}_{\pm 2}\gamma(\mathbf{n}) = \int \frac{d^3\mathbf{k}}{(2\pi)^3} {}_{\pm 2}\gamma(\mathbf{k}, \mathbf{n}). \quad (5.36)$$

Note that the definition differs from the Fourier transformation by the factor $\exp(i\mathbf{x} \cdot \mathbf{k})$. We obtain

$${}_{\pm}S(\mathbf{k}, \mathbf{n}) = - \int_0^{\bar{r}_s} d\bar{r} \frac{(\bar{r}_s - \bar{r})\bar{r}}{\bar{r}_s} k^2 (1 - \mu^2) \Psi(\mathbf{k}, \bar{r}) e^{i\bar{r}\mathbf{k} \cdot \mathbf{n}}, \quad (5.37)$$

and

$$\pm_2 T0(\mathbf{k}, \mathbf{n}, p) = -\frac{1}{2}(\mu \mp p)^2 C_p(\mathbf{k}, 0) \exp(ip2\phi), \quad (5.38)$$

$$\begin{aligned} \pm_2 T1(\mathbf{k}, \mathbf{n}, p) = & -\int_0^{\bar{r}_s} d\bar{r} \left(\frac{\bar{r}_s - \bar{r}}{\bar{r}_s \bar{r}} \right) \left((\mu \mp p)^2 - \frac{k^2 \bar{r}^2 (1 - \mu^2)^2}{2} - i2k\bar{r}(1 - \mu^2)(\mu \mp p) \right) \\ & \times C_p(\mathbf{k}, \bar{r}) e^{ip2\phi} e^{i\bar{r}\mathbf{k} \cdot \mathbf{n}}, \end{aligned} \quad (5.39)$$

$$\pm_2 T2(\mathbf{k}, \mathbf{n}, p) = \int_0^{\bar{r}_s} \frac{d\bar{r}}{\bar{r}} (-ik\bar{r}(1 - \mu^2)(\mu \mp p) + (\mu \mp p)^2) C_p(\mathbf{k}, \bar{r}) e^{ip2\phi} e^{i\bar{r}\mathbf{k} \cdot \mathbf{n}}, \quad (5.40)$$

$$\pm_2 T3(\mathbf{k}, \mathbf{n}, p) = -\frac{1}{2}(\mu \mp p)^2 C_p(\mathbf{k}, \bar{r}_s) \exp(ip2\phi) \exp(i\bar{r}_s \mathbf{k} \cdot \mathbf{n}), \quad (5.41)$$

where the details of the calculations are presented in appendix D.

Now, we apply the spin-lowering and -raising operator twice to $_{-2}\gamma(\mathbf{k}, \mathbf{n})$ and $_{+2}\gamma(\mathbf{k}, \mathbf{n})$, respectively. Note that, for a function given by ${}_s f(\theta, \phi) = e^{im\phi} {}_s \tilde{f}(\mu)$, the definitions of the operators given in equation (5.25) imply

$$\begin{aligned} \bar{\partial}^2 {}_2 f(\mu, \phi) &= \left(-\frac{\partial}{\partial \mu} + \frac{m}{1 - \mu^2} \right)^2 [(1 - \mu^2) {}_2 f(\mu, \phi)], \\ \bar{\partial}^2 {}_{-2} f(\mu, \phi) &= \left(-\frac{\partial}{\partial \mu} - \frac{m}{1 - \mu^2} \right)^2 [(1 - \mu^2) {}_{-2} f(\mu, \phi)]. \end{aligned} \quad (5.42)$$

Applying these relations with $m = 0$ for the scalar modes and $m = \pm 2$ for the tensor modes, and then turning powers of μ into powers of $-i\partial_x$ acting on $\exp(ix\mu)$, we obtain

$$\begin{aligned} \bar{\partial}^2 {}_2 \gamma(\mathbf{k}, \mathbf{n}) &= \int_0^{\bar{r}_s} d\bar{r} \left(\frac{\bar{r}_s - \bar{r}}{\bar{r}_s \bar{r}} \right) \hat{S}(x) \Psi(\mathbf{k}, \bar{r}) e^{ix\mu} + \sum_p \left[-6C_p(\mathbf{k}, 0) + C_p(\mathbf{k}, \bar{r}_z) \hat{T}_3(px_s) e^{ixs\mu} \right. \\ &\quad \left. + \int_0^{\bar{r}_z} d\bar{r} \left(\frac{\bar{r}_s - \bar{r}}{\bar{r}_s \bar{r}} \right) C_p(\mathbf{k}, \bar{r}) \hat{T}_1(x) e^{ix\mu} + \int_0^{\bar{r}_s} \frac{d\bar{r}}{\bar{r}} C_p(\mathbf{k}, \bar{r}) \hat{T}_2(px) e^{ix\mu} \right] (1 - \mu^2) e^{i2p\phi}, \end{aligned} \quad (5.43)$$

and

$$\begin{aligned} \bar{\partial}^2 {}_{-2} \gamma(\mathbf{k}, \mathbf{n}) &= \int_0^{\bar{r}_s} d\bar{r} \left(\frac{\bar{r}_s - \bar{r}}{\bar{r}_s \bar{r}} \right) \hat{S}(x) \Psi(\mathbf{k}, \bar{r}) e^{ix\mu} + \sum_p \left[-6C_p(\mathbf{k}, 0) + C_p(\mathbf{k}, \bar{r}_z) \hat{T}_3(-px_s) e^{ixs\mu} \right. \\ &\quad \left. + \int_0^{\bar{r}_z} d\bar{r} \left(\frac{\bar{r}_s - \bar{r}}{\bar{r}_s \bar{r}} \right) C_p(\mathbf{k}, \bar{r}) \hat{T}_1(x) e^{ix\mu} + \int_0^{\bar{r}_s} \frac{d\bar{r}}{\bar{r}} C_p(\mathbf{k}, \bar{r}) \hat{T}_2(-px) e^{ix\mu} \right] (1 - \mu^2) e^{i2p\phi}, \end{aligned} \quad (5.44)$$

where we have defined the operators

$$\hat{S}(x) = 4x^2 + x^4 + 8x^3 \partial_x + (12x^2 + 2x^4) \partial_x^2 + 8x^3 \partial_x^3 + x^4 \partial_x^4, \quad (5.45)$$

and

$$\begin{aligned} \hat{T}_1(x) &= -\frac{1}{2} [24 + 24x^2 + x^4 + (96x + 16x^3) \partial_x + (72x^2 + 2x^4) \partial_x^2 + 16x^3 \partial_x^3 + x^4 \partial_x^4], \\ \hat{T}_2(x) &= [12 + 5x^2 + (x^3 + 28x) \partial_x + 11x^2 \partial_x^2 + x^3 \partial_x^3] + i [-4x - x^3 - 6x^2 \partial_x - x^3 \partial_x^2], \\ \hat{T}_3(x) &= -\frac{1}{2} [12 - x^2 + 8x \partial_x + x^2 \partial_x^2] + i [4x + x^2 \partial_x]. \end{aligned} \quad (5.46)$$

Note that the operators $\hat{T}_2(x)$ and $\hat{T}_3(x)$ follow the conjugate relation $\hat{T}_i(x) = \hat{T}_i(-x) = \hat{T}_i^*(x)$, $i \in \{2, 3\}$. The operators $\hat{S}(x)$ and $\hat{T}_1(x)$ are purely real and remain invariant when changing $x \mapsto -x$. Furthermore, note that equations (5.42) coincide with those given in [32], while we chose slightly different definitions for the operators corresponding to tensor modes.⁵

Now, we can compute $a_{lm}^{\gamma\pm}(\mathbf{k})$ from equation (5.27) by applying equation (5.4) for the case $m = 0$ (scalar modes) and $m = \pm 2$ (tensor modes), and additionally also equation (5.19) to deal with the term evaluated at the observer position. This yields:

$$\begin{aligned} a_{lm}^{\gamma\pm}(\mathbf{k}) = & \delta_{l \geq 2} \delta_{m0} \sqrt{4\pi(2l+1)} \sqrt{\frac{(l-2)!}{(l+2)!}} i^l \int_0^{\bar{r}_s} d\bar{r} \left(\frac{\bar{r}_s - \bar{r}}{\bar{r}_s \bar{r}} \right) \Psi(\mathbf{k}, \bar{r}) S(l, x) \\ & - \sqrt{4\pi(2l+1)} i^l \sum_{p=\pm 1} \delta_{2m}^p C_p(\mathbf{k}) \left[-\frac{2}{5} T(\mathbf{k}, 0) \delta_{l2} + T(\mathbf{k}, \bar{r}_s) \hat{T}_3(\pm p x_s) \frac{j_l(x_s)}{x_s^2} \right. \\ & \left. + \int_0^{\bar{r}_s} d\bar{r} \left(\frac{\bar{r}_s - \bar{r}}{\bar{r}_s \bar{r}} \right) T_p(\mathbf{k}, \bar{r}) \hat{T}_1(x) \frac{j_l(x)}{x^2} + \int_0^{\bar{r}_s} \frac{d\bar{r}}{\bar{r}} T_p(\mathbf{k}, \bar{r}) \hat{T}_2(\pm p x) \frac{j_l(x)}{x^2} \right]. \quad (5.47) \end{aligned}$$

5.2.2 Calculation of the E- and B-mode angular power spectra

Having calculated $a_{lm}^{\gamma\pm}(\mathbf{k})$, we define

$$a_{lm}^{\mathcal{E}}(\mathbf{k}) \equiv \frac{1}{2} \left(a_{lm}^{\gamma+}(\mathbf{k}) + a_{lm}^{\gamma-}(\mathbf{k}) \right), \quad a_{lm}^{\mathcal{B}}(\mathbf{k}) = \frac{1}{2i} \left(a_{lm}^{\gamma+}(\mathbf{k}) - a_{lm}^{\gamma-}(\mathbf{k}) \right), \quad (5.48)$$

which yields

$$\begin{aligned} a_{lm}^{\mathcal{E}}(\mathbf{k}) = & \delta_{l \geq 2} \delta_{m0} \sqrt{4\pi(2l+1)} \sqrt{\frac{(l-2)!}{(l+2)!}} i^l \int_0^{\bar{r}_s} d\bar{r} \left(\frac{\bar{r}_s - \bar{r}}{\bar{r}_s \bar{r}} \right) \Psi(\mathbf{k}, \bar{r}) \hat{S}(l, x) \\ & - \sqrt{4\pi(2l+1)} i^l \sum_p \delta_{2m}^p C_p(\mathbf{k}) \left[-\frac{2}{5} T(\mathbf{k}, 0) \delta_{l2} + T(\mathbf{k}, \bar{r}_s) \text{Re} \hat{T}_3(l, x) \right. \\ & \left. + \int_0^{\bar{r}_s} d\bar{r} \left(\frac{\bar{r}_s - \bar{r}}{\bar{r}_s \bar{r}} \right) T(\mathbf{k}, \bar{r}) \hat{T}_1(l, x) + \int_0^{\bar{r}_s} \frac{d\bar{r}}{\bar{r}} T(\mathbf{k}, \bar{r}) \text{Re} \hat{T}_2(l, x) \right], \quad (5.49) \end{aligned}$$

and

$$a_{lm}^{\mathcal{B}}(\mathbf{k}) = -\sqrt{4\pi(2l+1)} i^l \sum_p \delta_{2m}^p C_p(\mathbf{k}) \left[T(\mathbf{k}, \bar{r}_s) \text{Im} \hat{T}_3(l, x) + \int_0^{\bar{r}_s} \frac{d\bar{r}}{\bar{r}} T(\mathbf{k}, \bar{r}) \text{Im} \hat{T}_2(l, x) \right], \quad (5.50)$$

where we have defined $\hat{S}(l, x) \equiv \hat{S}(x) j_l(x)$, and $\hat{T}_i(l, x) \equiv \hat{T}_i(x) (j_l(x)/x^2)$. While the operators $\hat{S}(x)$ and $\hat{T}_i(x)$ given in equations (5.45) and (5.46) are fairly complicated, the expressions for $\hat{S}(l, x)$ and $\hat{T}_i(l, x)$ can be simplified by using the differential and recursion relation of the spherical Bessel functions,

$$\left(\frac{1}{x} \frac{d}{dx} \right)^m \left(x^{l+1} j_l(x) \right) = x^{l-m+1} j_{l-m}(x), \quad j_{l+1}(x) = \frac{2l+1}{x} j_l(x) - j_{l-1}(x). \quad (5.51)$$

We obtain

$$\hat{S}(l, x) = \frac{(l+2)!}{(l-2)!} j_l(x), \quad (5.52)$$

⁵Compared to their notation, we have $\hat{T}_1(x) = -2\hat{Q}_3(x)$, $\hat{T}_2(x) = 2(\hat{Q}_2(x) + \hat{Q}_3(x))$ and $\hat{T}_3(x) = -\hat{Q}_1(x)/2$.

and

$$\begin{aligned}
\hat{T}_1(l, x) &= \frac{1}{2} (-l^4 - 2l^3 + l^2 + l(98 - 96x) + 192(-1 + x)) \frac{j_l(x)}{x^2} + 48(-1 + x) \frac{j_{l+1}(x)}{x}, \\
\text{Re } \hat{T}_2(l, x) &= (l^3 + 2l^2 - l - 2) \frac{j_l(x)}{x^2} - (l^2 + l - 2) \frac{j_{l+1}(x)}{x}, \\
\text{Re } \hat{T}_3(l, x) &= -\frac{1}{2} (l^2 + 3l + 2(1 - x^2)) \frac{j_l(x)}{x^2} + \frac{j_{l+1}(x)}{x},
\end{aligned} \tag{5.53}$$

and

$$\begin{aligned}
\text{Im } \hat{T}_2(l, x) &= -(l^2 x + l(6 - 5x) + 10x - 12) \frac{j_l(x)}{x^2} + 6(x - 1) \frac{j_{l+1}(x)}{x}, \\
\text{Im } \hat{T}_3(l, x) &= (2 + l) \frac{j_l(x)}{x} - j_{l+1}(x).
\end{aligned} \tag{5.54}$$

Note that the definition (5.48) indeed corresponds to the usual notion of E- and B-modes, i.e. that E-modes are invariant under parity transformation while B-modes change their sign. Under parity transformation, the basis vectors m_{\pm}^{α} transform into each other, $m_{\pm}^{\alpha} \mapsto m_{\mp}^{\alpha}$. Consequently, $\pm 2\gamma$ and $a_{lm}^{\gamma\pm}$ also transform into each other, $\pm 2\gamma \mapsto \mp 2\gamma$ and $a_{lm}^{\gamma\pm} \mapsto (-1)^l a_{lm}^{\gamma\mp}$, where the additional factor $(-1)^l$ is due to the parity transformation property of the spin-weighted spherical harmonics,

$${}_s Y_{lm} \mapsto (-1)^l {}_{-s} Y_{lm}. \tag{5.55}$$

Hence, we have $a_{lm}^{\mathcal{E}} \mapsto (-1)^l a_{lm}^{\mathcal{E}}$ and $a_{lm}^{\mathcal{B}} \mapsto -(-1)^l a_{lm}^{\mathcal{B}}$, and

$$\sum_{l,m} a_{lm}^{\mathcal{E}} Y_{lm} \mapsto \sum_{l,m} a_{lm}^{\mathcal{E}} Y_{lm}, \quad \sum_{l,m} a_{lm}^{\mathcal{B}} Y_{lm} \mapsto -\sum_{l,m} a_{lm}^{\mathcal{B}} Y_{lm}, \tag{5.56}$$

which means that E- and B-modes can indeed be classified by their parity-transformation properties.

Having obtained the expressions for $a_{lm}^{\mathcal{E}}(\mathbf{k})$ and $a_{lm}^{\mathcal{B}}(\mathbf{k})$, we can finally derive the expressions for $C^X(l)$ for $X \in \{\mathcal{E}, \mathcal{B}\}$:

$$\begin{aligned}
C^X(l) &= \frac{1}{2l+1} \sum_{m=-l}^l \int \int \frac{d^3 \mathbf{k}}{(2\pi)^3} \frac{d^3 \mathbf{k}'}{(2\pi)^3} \langle a_{lm}^X(\mathbf{k}) (a_{lm}^X(\mathbf{k}'))^* \rangle \\
&= \frac{2}{\pi} \frac{(l+2)!}{(l-2)!} \int dk k^2 P_{\zeta}(k) (\mathcal{S}_l^X(k))^2 + \frac{1}{8\pi} \int dk k^2 P_T(k) (\mathcal{T}_l^X(k))^2,
\end{aligned} \tag{5.57}$$

where

$$\mathcal{S}_l^{\mathcal{E}}(k) = \delta_{l \geq 2} \int_0^{\bar{r}_s} d\bar{r} \left(\frac{\bar{r}_s - \bar{r}}{\bar{r}_s \bar{r}} \right) D_{\Psi}(\bar{r}) j_l(x), \quad \mathcal{S}_l^{\mathcal{B}}(k) = 0, \tag{5.58}$$

and

$$\begin{aligned}
\mathcal{T}_l^{\mathcal{E}}(k) &= \delta_{l \geq 2} \left[-\frac{2}{5} T(k, 0) \delta_{l2} + T(k, \bar{r}_s) \text{Re } \hat{T}_3(l, x_s) + \int_0^{\bar{r}_s} d\bar{r} \left(\frac{\bar{r}_s - \bar{r}}{\bar{r}_s \bar{r}} \right) T(k, \bar{r}) \hat{T}_1(l, x) \right. \\
&\quad \left. + \int_0^{\bar{r}_s} \frac{d\bar{r}}{\bar{r}} T(k, \bar{r}) \text{Re } \hat{T}_2(l, x) \right], \\
\mathcal{T}_l^{\mathcal{B}}(k) &= \delta_{l \geq 2} \left[T(k, \bar{r}_s) \text{Im } \hat{T}_3(l, x_s) + \int_0^{\bar{r}_s} \frac{d\bar{r}}{\bar{r}} T(k, \bar{r}) \text{Im } \hat{T}_2(l, x_s) \right].
\end{aligned} \tag{5.59}$$

The cross-correlation between the E- and B-modes vanishes due to their different behavior under parity transformation. Note that our results for the tensor mode contribution to $C^X(l)$ coincide with the expression calculated by Schmidt & Jeong in [32].⁶

Applying a more general distribution function $n(\bar{r})$ instead of a sharp source redshift $\delta(\bar{r} - \bar{r}_z)$, i.e. performing the calculations for the integrated shear components Γ_i given in equation (2.21), the operators $\mathcal{S}_l^X(k)$ and $\mathcal{T}_l^{\gamma X}(k)$, where $X \in \{\mathcal{E}, \mathcal{B}\}$, need to be replaced by

$$\mathcal{S}_l^E(k) = \delta_{l \geq 2} \int_0^{\bar{r}_S} d\bar{r} g(\bar{r}) D_\Psi(\bar{r}) j_l(x), \quad \mathcal{S}_l^B(k) = 0, \quad (5.60)$$

and

$$\begin{aligned} \mathcal{T}_l^E(k) = & \delta_{l \geq 2} \left[-\frac{1}{5} T(k, 0) \delta_{l2} + \int_0^{\bar{r}_S} d\bar{r} n(\bar{r}) T(k, \bar{r}) \text{Re} \hat{T}_3(l, x) \right. \\ & \left. + \int_0^{\bar{r}_S} d\bar{r} g(\bar{r}) T(k, \bar{r}) \hat{T}_1(l, x) + \int_0^{\bar{r}_S} d\bar{r} h(\bar{r}) T(k, \bar{r}) \text{Re} \hat{T}_2(l, x) \right], \\ \mathcal{T}_l^B(k) = & \delta_{l \geq 2} \left[\int_0^{\bar{r}_S} d\bar{r} T(k, \bar{r}) \text{Im} \hat{T}_3(l, x) + \int_0^{\bar{r}_S} d\bar{r} h(\bar{r}) T(k, \bar{r}) \text{Im} \hat{T}_2(l, x) \right]. \end{aligned} \quad (5.61)$$

5.3 All-sky cross power spectrum of E-modes and δD

The cross power spectrum between δD and the shear B-modes vanishes due to their different parity transformation properties. With the expressions for the scalar and tensor mode contributions to $a_{lm}^{\delta D}(\mathbf{k})$ given in equations (5.9) and (5.17) and the expression for $a_{lm}^{\mathcal{E}}(\mathbf{k})$ given in equation (5.49), we immediately obtain the expression for the cross power spectrum $C^{\delta D \mathcal{E}}(l)$,

$$\begin{aligned} C^{\delta D \mathcal{E}}(l) = & \frac{1}{2l+1} \sum_{m=-l}^l \int \int \frac{d^3 \mathbf{k}}{(2\pi)^3} \frac{d^3 \mathbf{k}'}{(2\pi)^3} \langle a_{lm}^{\delta D}(\mathbf{k}) (a_{lm}^{\mathcal{E}}(\mathbf{k}'))^* \rangle \\ = & \frac{1}{8\pi} \sqrt{\frac{(l+2)!}{(l-2)!}} \int dk k^2 P_T(k) \mathcal{T}_l^{\delta D \mathcal{E}}(k) + \frac{2}{\pi} \sqrt{\frac{(l+2)!}{(l-2)!}} \int dk k^2 P_\zeta(k) \mathcal{S}_l^{\delta D \mathcal{E}}(k), \end{aligned} \quad (5.62)$$

where

$$\mathcal{S}_l^{\delta D \mathcal{E}}(k) = \mathcal{S}_l^{\delta D}(k) \mathcal{S}_l^{\mathcal{E}}(k), \quad \mathcal{T}_l^{\delta D \mathcal{E}}(k) = \mathcal{T}_l^{\delta D}(k) \mathcal{T}_l^{\mathcal{E}}(k). \quad (5.63)$$

These relations also apply if δD and \mathcal{E} are replaced by ΔD and E , i.e. for a general source redshift distribution. Note that, for the same reasons as discussed in section 4.3, $C^{\delta D \mathcal{E}}(l)$ is not equal to $C^{\mathcal{E}}(l)$. However, when taking into account only the term $\sim l(l+1)$ in equation (5.10) arising from the standard lensing convergence κ , we obtain the relation

$$C^{\mathcal{E}}(l) = \frac{(l+2)(l-1)}{(l+1)l} C^\kappa(l) = -\sqrt{\frac{(l+2)(l-1)}{(l+1)l}} C^{\kappa \mathcal{E}}(l), \quad (5.64)$$

which is valid for all $l \geq 2$ and recovers the relation between $C^{\mathcal{E}}(l)$ and $C^\kappa(l)$ derived in [33]. This corresponds to the Limber-approximated relation $C^{\mathcal{E}}(l) = C^\kappa(l) = -C^{\kappa \mathcal{E}}(l)$ up to the factors of l , which arise from the fact that $C^\kappa(l)$ is derived from a spin-0 quantity, while $C^{\mathcal{E}}(l)$ corresponds to the spin-2 quantities $\pm 2\gamma$.

⁶Note that our results for $\mathcal{T}_l^{\gamma E}(k)$ and $\mathcal{T}_l^E(k)$ differ from those in [32] by an overall factor of 2, which arise from the different definitions of the tensor mode perturbations, $h_{\alpha\beta} = 2C_{\alpha\beta}$.

6 Numerical results for the angular power spectra

In this section, we numerically evaluate the general relativistic weak lensing angular power spectra. We focus our discussion mainly on the magnification angular power spectrum (section 6.1), as it is most affected by general relativistic effects. In section 6.2, we also show our numerical results for the shear E-mode angular power spectrum and their cross angular power spectrum with the magnification, where we comment on the impacts of both the Limber approximation and general relativistic effects.

For these numerical evaluations, we apply the Euclid-like redshift distribution function given in equation (2.30), and compare the resulting angular power spectra to a sharp redshift distribution with all sources located at $z_s = 2$. For a real survey, any source redshift distribution (possibly split into more narrow redshift bins in the case of tomographic lensing) will always have some finite width. Nevertheless, the theoretical case of a single source redshift serves to demonstrate the dependence of the relativistic corrections on the width of the source redshift distribution. We compute these angular power spectra by using the Limber approximation in section 4 and, to analyze the accuracy of this approximation, also by using the all-sky precise expressions calculated in section 5. All quantities are evaluated for the angular multipoles $l = 2, 3, \dots, 100$ (apart from the small and rapidly falling tensor mode contribution in figure 8 which we only plot for $l = 2, 3, \dots, 50$). Note that, despite the appearance of the plots at low l , these values are discrete.

We calculate the contribution of scalar modes by first evaluating the matter power spectrum $P_{m,0}$ at $a_0 = 1$, and then use the relations in a Λ CDM universe given in section 3.1 to obtain the power spectra of scalar perturbations at any scale factor a . For definiteness, we assume $H_0 = 67.4$ km/s/Mpc for the Hubble constant, $\Omega_b h^2 = 0.0224$ and $\Omega_{cdm} h^2 = 0.12$ for the baryonic and dark matter density, $n_s = 0.966$ for the scalar spectral index and $A_s = 2.1 \times 10^{-9}$ for the scalar amplitude at the pivot scale $k_0 = 0.05$ /Mpc, consistent with the Planck 2018 results [34]. For the contribution of the tensor modes, we use the relations given in section 3.2, where we assume a value of $r = 0.1$ at $k_0 = 0.002$ /Mpc for the tensor-to-scalar ratio defined as $A_T = r A_s$ at pivot scale k_0 . This is consistent with the upper bounds set by the Planck 2018 results [35], and yields the tensor amplitude $A_T = 2.34 \times 10^{-10}$ at $k_0 = 0.002$ /Mpc and the tensor spectral index $n_T = -r/8 = -0.0125$ as expected from single-field inflation.

6.1 Angular power spectrum of the magnification

First, we numerically evaluate and analyze the angular power spectrum of ΔD using the Limber approximation, illustrating our results in figure 2. In the left panel, we plot the total angular power spectrum $C^{\Delta D}(l)$ (black), and its main contribution from the standard lensing convergence $C^K(l)$ (blue). For that, we apply both the Euclid-like source redshift distribution in equation (2.30) (solid) and the sharp distribution with all sources located at $z_s = 2$ (dashed).

We see that, for both these cases, the angular power spectra of ΔD and K are essentially identically at $l \gtrsim 20$, while there is a significant deviation at larger angular scales. These are caused by the additional relativistic contributions to ΔD given in equation (2.23), more precisely the distortions in radial and redshift coordinate Δr and Δz and the potential Ψ_s at the source integrated over the redshift distribution. Their individual angular power spectra are shown in the right panel of figure 2, multiplied by a factor l^2 to better illustrate the quickly falling additional contributions. Note that there is no dashed orange curve, since

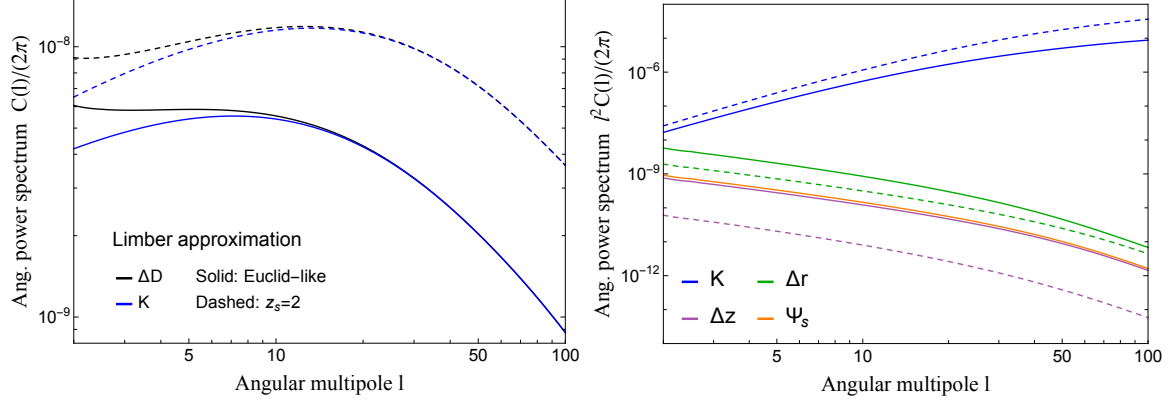


Figure 2: The left panel shows the angular power spectra of the magnification ΔD and the standard lensing convergence K as a function of multipole moment l , evaluated using the Limber approximation. The right panel shows the contributions of the additional terms Δr , Δz and Ψ_s , comparing them to the contribution of K , where the angular power spectra have been multiplied by l^2 . For both panels, the solid lines belong to the Euclid-like redshift distribution and the dashed lines to a unique source redshift $z_s = 2$.

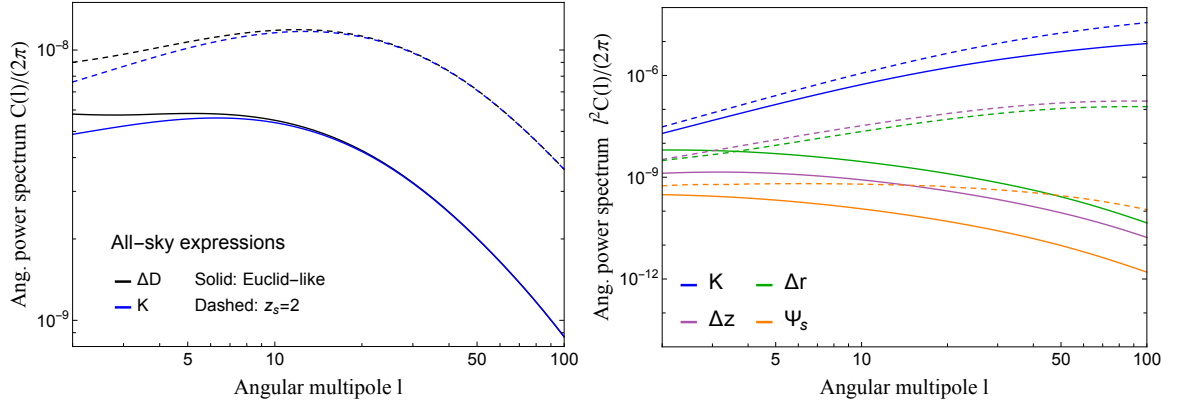


Figure 3: Same as figure 2, but using the precise all-sky expressions of section 5 instead of the Limber approximation.

the Limber approximation cannot account for any terms evaluated at a sharp redshift, as explained in section 4. Furthermore, note that for Δr and Δz our numerical calculations yield a higher angular power spectrum for the Euclid-like redshift distribution than for the unique source redshift $z_s = 2$, which seems counter-intuitive as the peak redshift of the Euclid-like distribution is lower than 2. This is simply a consequence of the fact that the terms evaluated at the source position in equations (2.11) and (2.12) for the non-integrated quantities δr and δz have to be omitted for the case $z_s = 2$.

Looking at the contribution of Δz , another noticeable feature is that for the Euclid-like redshift distribution, the angular power spectrum of Δz is almost identical to the angular power spectrum of the potential Ψ_s at the source position. The distortion in redshift Δz given in equation (2.26) has, apart from observer terms, contributions from the potential and line-of-sight velocity at the source and from changing potentials along the photon path.

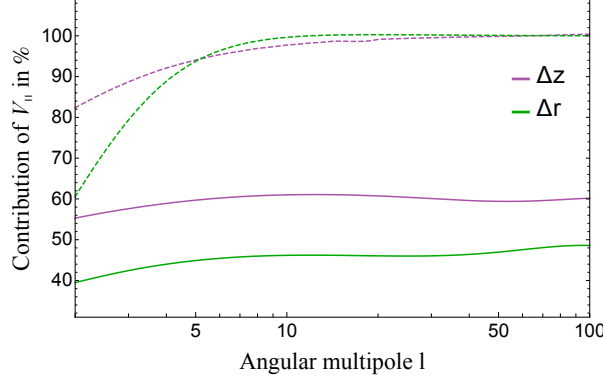


Figure 4: Fractional contribution of the line-of-sight velocity V_{\parallel} to the angular power spectra of Δr and Δz , where solid and dashed lines have the same meaning as in figure 2.

As the Limber approximation does not account for the line-of-sight velocity, and the contribution from changing potentials is small, this indeed leaves the potential at the source as the dominant term in the power spectrum of Δz . Note that the contribution of the source potential to Δz given by equation (2.26) and the additional source potential term appearing separately in equation (2.23) are two distinct terms which both contribute to the total ΔD .

Apart from the fact that the Limber approximation cannot account for terms evaluated at a unique redshift or for the line-of-sight velocity, it is also based on assumptions involving a flat sky geometry, which break down on large angular scales. To evaluate the error made by applying this approximation, particularly on large scales, we numerically calculate the angular power spectrum of ΔD and its individual components using the precise all-sky expressions given in section 5. We illustrate our results in figures 3–7 for scalar modes, and in figure 8 for tensor modes.

Figure 3 shows the angular power spectrum of ΔD and its individual components in the same format as figure 2, but using the precise all-sky expressions instead of the Limber approximation. Now, the plot on the right panel also contains a dashed orange line for the angular power spectrum of the source term Ψ_s evaluated at a unique source redshift $z_s = 2$. Comparing it to the solid orange line, we see that the distribution of the source terms falls off faster for a continuous redshift distribution. The same is true for the angular power spectra of Δr and Δz . As illustrated in figure 4, they both have a major contribution from the line-of-sight velocity V_{\parallel} that has already been studied in [4]. This contribution is particularly dominant for a unique redshift $z_s = 2$, while integrating over a broader redshift distribution reduces it. For a Euclid-like redshift distribution, we conclude that considering only the line-of-sight velocity in addition to the convergence is not sufficient, as it contributes to only about half of the signal from general relativistic corrections.

Another noticeable feature of the contributions of Δr and Δz is that, while $C^{\Delta r}(l)$ is higher than $C^{\Delta z}(l)$ for the Euclid-like redshift distribution, it is the opposite for a unique source redshift $z_s = 2$. This is explained by the fact that the source velocity term in δr contributes to δD with a factor $1/(\mathcal{H}_s \bar{r}_s)$, which is considerably larger than one for low redshifts, but drops below one at $z \approx 1.6$. Hence, $C^{\Delta r}(l)$ will be larger than $C^{\Delta z}(l)$ for any survey probing mainly at $z \lesssim 1.6$, and smaller otherwise.

In figure 5, we compare the precise all-sky angular power spectra (solid) with the Limber-

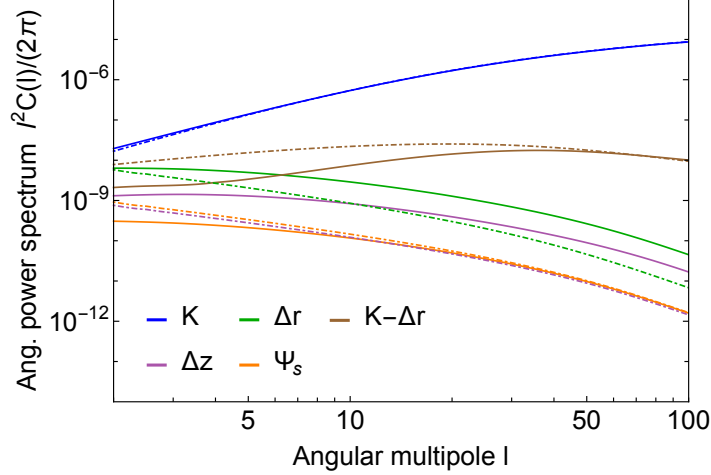


Figure 5: Comparison between the all-sky results (solid) and the Limber approximation (dot-dashed) for the angular power spectra of K , Δz , Δr and Ψ_s , and the cross-power spectrum of K and Δr multiplied by a factor of -2 . A Euclid-like redshift distribution is applied for all lines. Note that the total angular power spectrum of ΔD is not plotted as it would mostly overlap with the result for K .

approximated results (dot-dashed) for the Euclid-like redshift distribution function. For the angular power spectra of K and Ψ_s , the precise and Limber-approximated results coincide well on large l . This is not true for Δz and Δr as they have major contributions from the line-of-sight velocity, which is not accounted for in the Limber approximation. Furthermore, the angular power spectrum of K is at low l larger for the all-sky calculations than for the Limber-approximation, which is better illustrated in the left panel of figure 6. The same is true for the relativistic corrections Δz and Δr . Nevertheless, the left panel of figure 6 shows that for the total ΔD , the result at low l for the Euclid-like redshift distributions functions is lower for the all-sky calculations. To explain this, we have included an additional quantity in figure 5: the cross angular power spectrum $C^{K\Delta r}(l)$, multiplied by a factor -2 to properly account for its contribution to $C^{\Delta D}(l)$. This quantity is indeed reduced for the all-sky calculations due to the negative cross angular power spectrum between K and the source velocity contribution to Δr at low l . This also helps to explain the right panel of figure 6, which shows that the deviation of $C^{\Delta D}(l)$ from its main contribution $C^K(l)$ is in fact, despite the contribution of the source velocity, lower for the precise results than for the Limber approximation.

The left panel of figure 6 further shows that the error of the Limber approximation is lower for the fully relativistic magnification ΔD than for the standard convergence K , indicating that the inaccuracies of this approximation partly compensate each other when all contributions are included. Indeed, for a Euclid-like redshift distribution (solid black line), the error of using the Limber approximation is below 2% for all $l \geq 3$ (considering the absolute value of the error), and drops below 1% at $l \approx 50$. The right panel of figure 6 shows that, while at very low l omitting other contributions to ΔD apart from K induces a large error, it falls off and becomes negligible fast. In particular, for the precise calculations of a Euclid-like survey (solid gray curve), the deviation of $C^{\Delta D}(l)$ from $C^K(l)$ drops below 1% at $l = 19$, and is completely negligible at $l = 100$ ($\approx 0.08\%$).

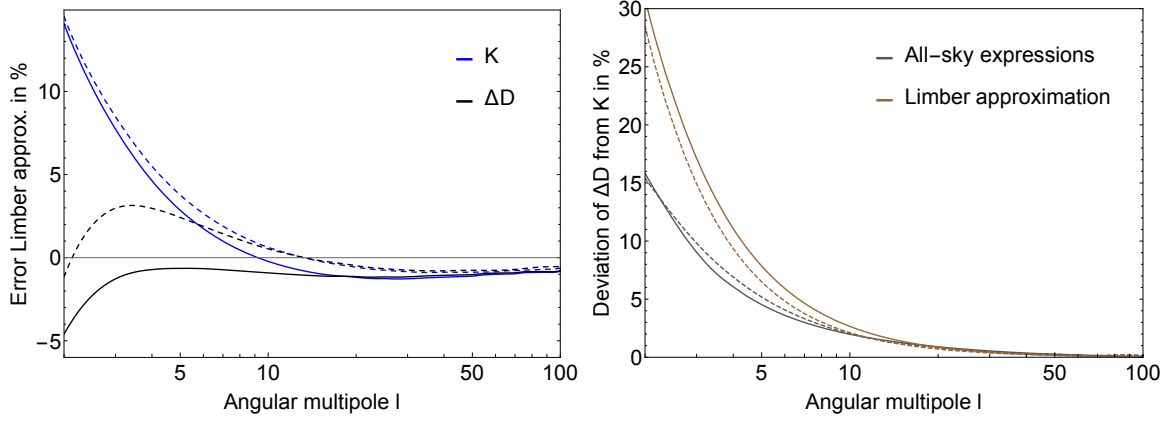


Figure 6: Accuracy of the Limber approximation and impact of relativistic effects. The left panel shows the fractional deviation $(C_{\text{all-sky}}^X(l) - C_{\text{Limb.}}^X(l))/C_{\text{all-sky}}^X(l)$ from the precise results when using the Limber approximation for the angular power spectrum of $X = \Delta D, K$. The right panel shows the fractional deviation $(C^{\Delta D}(l) - C^K(l))/C^{\Delta D}(l)$ of the total angular power spectrum $C^{\Delta D}(l)$ from $C^K(l)$. For both panels, dashed and solid lines have the same meaning as in figure 2.

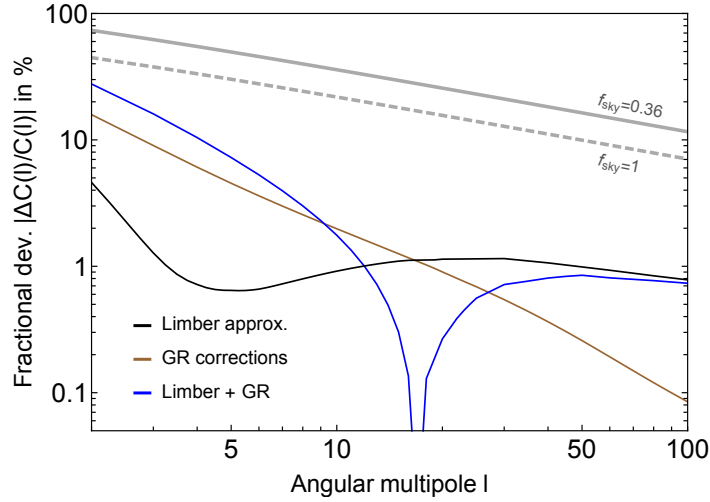


Figure 7: Fractional deviation caused by the Limber approximation (black), neglecting general relativistic effects (i.e. considering K only; brown), and their combined error when both simplifications are made (blue). All these three curves correspond to a Euclid-like redshift distribution. Additionally, we also plot the cosmic variance for Euclid covering 36% of the sky (solid gray), and an idealized survey covering the whole sky (dashed gray). Note that we chose a logarithmic scale for the fractional deviation to better compare errors with different orders of magnitude, and that we therefore depict absolute values.

Finally, to examine the significance of general relativistic effects for a Euclid-like survey we compare it (along with the error from the Limber approximation) to cosmic variance given by $\Delta C(l)/C(l) = 1/\sqrt{f_{\text{sky}}(2l+1)}$ in figure 7. Here, f_{sky} is the fraction of the sky covered by

the survey, i.e. $f_{\text{sky}} = 0.36$ for Euclid (expected to cover 15,000 square degrees). Additionally, we include the cosmic variance for an idealized all-sky survey, $f_{\text{sky}} = 1$, representing the theoretical limit for a survey's information content. At $l \geq 10$, the error made by neglecting general relativistic effects is at least one order or magnitude below cosmic variance, and thus would have a negligible effect on the error bars for cosmological parameter estimations. Only on the largest scales, $l < 10$, they gain significance, although still being below cosmic variance. Nevertheless, general relativistic effects should be taken into account on these largest scales to ensure optimal cosmological parameter constraints, especially since different errors (such as the combined error from assuming the Limber approximation and neglecting general relativistic effects given by the blue curve) can add up on those scales.

Note that while figures 2–7 only show the multipoles starting from $l = 2$, the magnification ΔD also has a dipole ($l = 1$) and monopole ($l = 0$) contribution. Indeed, the dipole of ΔD is, with $C^{\Delta D}(l = 1) \approx 1.5 \times 10^{-5}$ for a Euclid-like distribution, three orders of magnitude larger than the subsequent multipole $l = 2$. This large dipole arises due to the observer's velocity, contributing to K , Δz and Δr . For the monopole $l = 0$, we find that the standard convergence K and also the additional contributions Δz , Δr and Ψ_s yield a diverging result. However, this divergence in fact cancels out when considering the full observable ΔD , yielding a finite value of $C^{\Delta D}(l = 0) \approx 7.2 \times 10^{-8}$. This cancellation can be shown analytically by considering equation (5.10) for $S_l^{\delta D}(k)$ with $l = 0$ in the infrared limit $k \rightarrow 0$. Noting that $\lim_{x \rightarrow 0} j_0(x) = 1$ and $\lim_{x \rightarrow 0} j'_0(x) = 0$, and using the relation between D_Ψ , D_V and D'_V stated in equation (3.7), one obtains $S_0^{\delta D}(k \rightarrow 0) = 0$. Indeed, the cancellation of infrared divergences in the luminosity distance (recall that δD described the distortion in the angular diameter distance and equivalently in the luminosity distance) and its relation to the equivalence principle have already been discussed in [23].

Finally, let us also comment on the tensor mode contribution to the magnification angular power spectrum illustrated in figure 8. It shows that their contribution is even for the lowest l several orders of magnitude below the scalar mode contribution, and the general relativistic corrections further reduce the signal. Hence, given the Planck 2018 constraint for the tensor-to-scalar ratio, a detection of primordial gravitational waves through magnification effects is impossible. Note that figure 8 also shows that the Limber-approximated and all-sky results do not converge for large l . This corresponds to the conclusion in [36] that the Limber approximation is simply not applicable to tensor modes with their rapidly oscillating transfer function. Furthermore, note that for the tensor contribution to $C^K(l)$, we did not plot the result for $l = 2$. Indeed, tensor modes would lead to an unphysical divergence in $C^K(l = 2)$, similarly to how scalar modes lead to an equally unphysical divergence in $C^K(l = 0)$. For the full magnification ΔD however, this divergence is vanishing, as equation (5.18) yields $\mathcal{T}_l^{\delta D}(k \rightarrow 0) = 0$.

6.2 Shear E-mode angular power spectrum and shear-magnification cross power spectrum

Unlike the convergence K , which needs to be replaced by the distortion in the luminosity distance ΔD in a fully-relativistic approach, the cosmic shear E-modes do not obtain any additional scalar contribution from relativistic corrections. However, we can evaluate the impact of the Limber approximation, as shown in figure 9. We see that, while the error made by using this approximation is substantial at $l \leq 10$, it falls off fast at these very large angular scales and is below 2% for all $l > 10$. However, it then continues to fall off rather slowly. For a Euclid-like source redshift distribution, the error is below 1% only at $l > 70$.

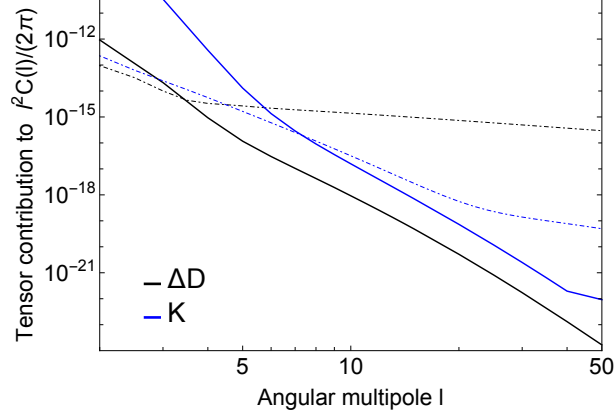


Figure 8: Tensor mode contribution to $C^{\Delta D}(l)$ and $C^K(l)$, where the solid lines correspond to all-sky calculations and dotted-dashed lines to the Limber approximation.

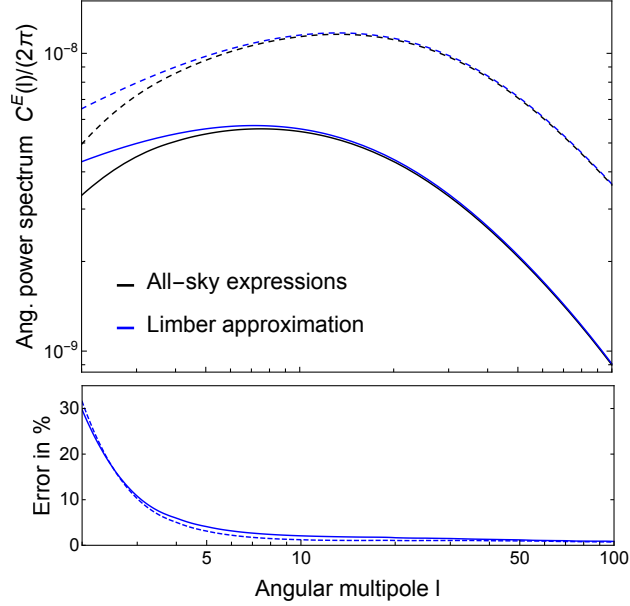


Figure 9: Accuracy of the Limber approximation for the shear E-mode power spectrum. The top panel shows the shear E-mode angular power spectrum using both the Limber approximation and precise all-sky expressions, where dashed and solid lines have the same meaning as in figure 2. The bottom panel shows the fractional error of the Limber approximation with respect to the all-sky results.

This is well compatible with [8], where it was concluded that the considered approximations would lead to an error of $> 1\%$ at $l < 40$ for a Euclid-like survey. For previous surveys, the impact of the Limber approximation was negligible due to the comparably small survey area (e.g. 1,500 square degrees of total survey area for KiDS, corresponding to $f_{\text{sky}} = 0.036$ [5]) and the therefore large cosmic variance. However, as concluded in [10], upcoming surveys

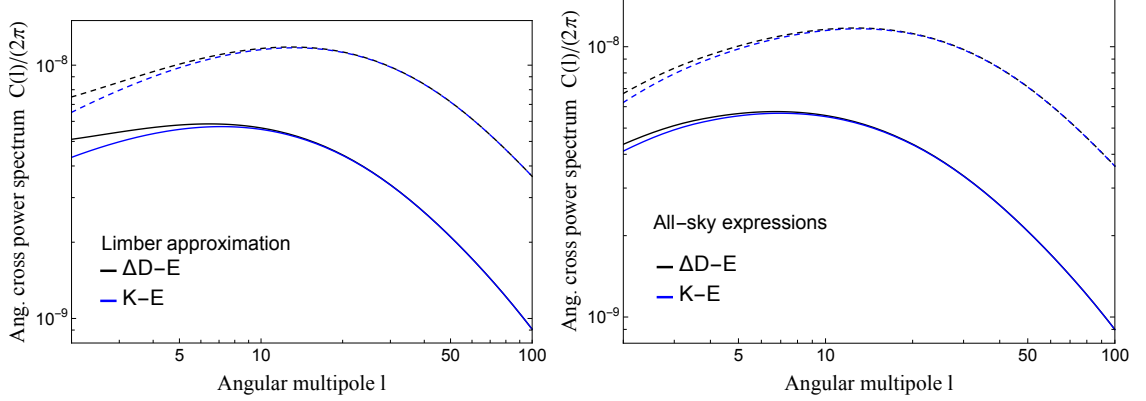


Figure 10: Cross angular power spectrum of ΔD and the shear E-modes for the Limber approximation (left panel) and the precise results (right panel). Dashed and solid lines have the same meaning as in figure 2. Apart from the total $C^{\Delta DE}(l)$, we also plot its main contribution $-C^{KE}(l)$, with a minus due to the opposite sign conventions of ΔD and K .

such as Euclid require a more precise theoretical modeling.⁷

Apart from scalar modes, tensor modes from primordial gravitational waves in principle also contribute to the shear E-modes and generate a small B-mode signal. For this tensor mode contribution, we obtain numerical results compatible with figure 1 and figure 2 in [32] (although around a factor of 2 smaller due to the even smaller tensor-to-scalar ratio assumed here). Hence, this tensor mode lensing signal is completely negligible. As discussed [32], tensor modes would contribute to cosmic shear more strongly through intrinsic alignment than through lensing. However, even the intrinsic alignment signal appears too low for a detection to be feasible. We conclude that, unless there is any non-standard physics e.g. generating vector modes through cosmic strings, cosmic shear can be fully described by scalar modes only.

When measuring both magnification effects and cosmic shear, one can evaluate the cross spectrum $C^{\Delta DE}(l)$ additionally to the individual E-mode and magnification angular power spectra. In figure 10, we show our numerical results for this quantity, again both for a Euclid-like redshift distribution and a unique source redshift $z_s = 2$, and using both the Limber approximation and precise expressions. Apart from plotting the total $C^{\Delta DE}(l)$, we also provide the results for $C^{KE}(l)$.

Not surprisingly, the left and right panels of figure 10 look similar to the left panels of figure 2 and 3, respectively. Indeed, the angular power spectra $C^K(l)$ and $C^{KE}(l)$, involving only the main contribution K , differ only by factors of l as given in equation (5.64). Consequently, figure 11 also leads to similar conclusions as figure 6. In particular, the error of the Limber approximation (left panel) falls off fast at the largest scales $l \lesssim 10$, and then continues to fall off only slowly, dropping below 1% at $l \gtrsim 60$. Finally, while the right panel of figure 11 looks at first similar to the right panel of figure 6, the error made by neglecting additional contributions to ΔD other than K is now even smaller (below 1% for all $l \geq 10$), as only one of the two correlated quantities is affected. Hence, the contribution of relativistic corrections

⁷Due to the low computational speed associated with all-sky calculations, they recommend to rather use the sufficiently precise second-order extended Limber approximation presented in [11].

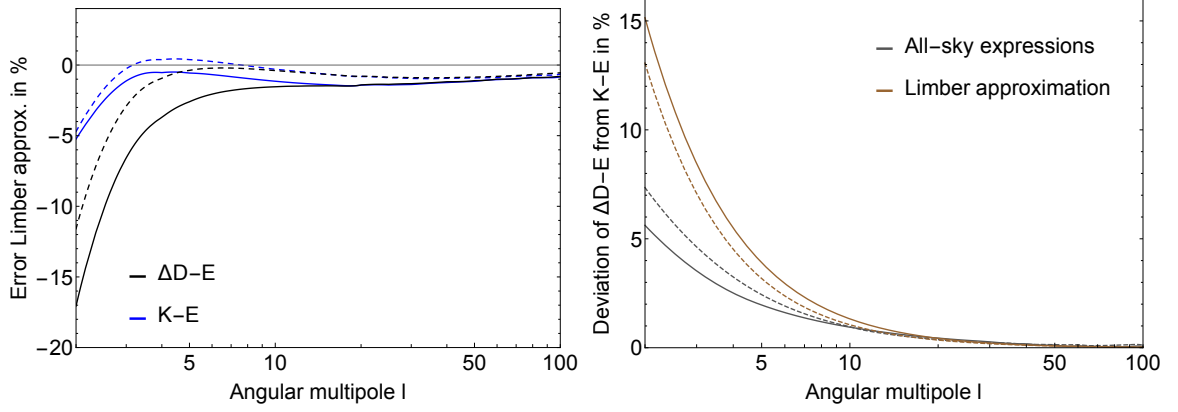


Figure 11: Accuracy of the Limber approximation and impact of relativistic effects in the angular cross power spectrum. The left panel shows the fractional deviation $(C_{\text{Limb.}}^{XE}(l) - C_{\text{all-sky}}^{XE}(l))/C_{\text{all-sky}}^{XE}(l)$ from the precise results when using the Limber approximation for the angular power spectrum of $X = \Delta D, K$. The right panel shows the fractional deviation $(C^{\Delta DE}(l) + C^{KE}(l))/C^{\Delta DE}(l)$, with a plus instead of a minus due to the opposite sign conventions of ΔD and K . For both panels, dashed and solid lines have the same meaning as in figure 2.

to the cross angular power spectrum between shear E-modes and the magnification is well below cosmic variance on all scales.

7 Conclusion

In this work, we have for the first time presented the analytical expression of the lensing magnification angular power spectrum including all general relativistic contributions arising from linear-order scalar and tensor modes. To obtain the analytical expressions, we have applied the Limber approximation based on a flat-sky geometry, and since it breaks down on the large angular scales where general relativistic effects become important, we have also used the precise approach based on the spherical harmonics decomposition. In addition to the magnification angular power spectrum, we have also given the expressions for the shear E- and B-mode angular power spectra, and the shear-magnification cross power spectrum which is affected by the relativistic corrections to the magnification.

Our numerical calculations show that, for a Euclid-like source redshift distribution, relativistic effects lead to corrections of more than one percent in the magnification angular power spectrum at large angular scales $l \leq 20$. In particular, we have shown that taking into account only the source velocity in addition to the standard lensing convergence is not sufficient, as it only accounts for about half of the additional signal from relativistic effects. For the cross angular power spectrum between shear E-modes and the magnification, general relativistic corrections are above one percent only for $l \leq 10$. Regarding the Limber approximation, we conclude that it leads to errors of more than one percent at $l \lesssim 60$, compatible with previous results (see e.g. [8]). Our numerical calculations of the tensor mode contribution show that, with the upper bound for the tensor-to-scalar ratio set by the Planck 2018 results, they are completely negligible even at the largest scales.

While general relativistic corrections to the standard lensing formalism are at least one order of magnitude below cosmic variance for $l \geq 10$, they gain significance at the largest scales $l < 10$. In particular, the error from neglecting general relativistic effects is enhanced when combined with the Limber approximation, showing that an accurate modeling of the magnification is necessary when analyzing large-scale data. Moreover, we also want to point out that general relativistic effects should not only be seen as corrections to standard effects, but also as an important cosmological probe themselves. In particular, as pointed out in [4], the standard lensing convergence is determined by the sum of the Bardeen potentials $\Phi + \Psi$, but the additional general relativistic corrections break the degeneracy between them. While we did not distinguish between these two potentials in this work, as general relativity with no anisotropic stress component predicts $\Phi = \Psi$, modified gravity theories can lead to deviations from this assumption.

We conclude that, although general relativistic effects in weak lensing angular power spectra are negligible at small scales ($l \geq 10$) compared to the cosmic variance, they should be taken into account at the largest scales $l < 10$ to optimally interpret the data from future surveys. Moreover, they provide a test for theories of gravity and therefore deserve the attention from both the theoretical and observational community.

Acknowledgments

We thank Fulvio Scaccabarozzi and Giuseppe Fanizza for useful discussions. We acknowledge support by the Swiss National Science Foundation (SNF CRSII5_173716), and J.Y. is further supported by a Consolidator Grant of the European Research Council (ERC-2015-CoG grant 680886).

A Vector calculus identities in spherical coordinates

Observed source positions on the sky are usually described by spherical coordinates – a radial coordinate $\bar{r}(z)$ associated to the observed redshift z and observed angular coordinates (θ, ϕ) . Therefore, we naturally describe observables such as the magnification and the shear components using angular coordinates. Here, we review some vector calculus identities in spherical coordinates that are fundamental for this work. First of all, the line-of-sight direction n^α specified by the observed angles θ and ϕ is given by

$$\mathbf{n} = n^\alpha(\theta, \phi) = \begin{pmatrix} \sin \theta \cos \phi \\ \sin \theta \sin \phi \\ \cos \theta \end{pmatrix}. \quad (\text{A.1})$$

Introducing two vectors orthonormal to n^α ,

$$\theta^\alpha(\mathbf{n}) = \theta^\alpha(\theta, \phi) = \begin{pmatrix} \cos \theta \cos \phi \\ \cos \theta \sin \phi \\ -\sin \theta \end{pmatrix}, \quad \phi^\alpha(\mathbf{n}) = \phi^\alpha(\theta, \phi) = \begin{pmatrix} -\sin \phi \\ \cos \phi \\ 0 \end{pmatrix}, \quad (\text{A.2})$$

we can write the gradient as

$$\frac{\partial}{\partial x^\alpha} = n_\alpha \frac{\partial}{\partial \bar{r}} + \frac{1}{\bar{r}} \hat{\nabla}_\alpha, \quad \hat{\nabla}_\alpha \equiv \theta_\alpha \frac{\partial}{\partial \theta} + \phi_\alpha \frac{1}{\sin \theta} \frac{\partial}{\partial \phi}, \quad (\text{A.3})$$

where we refer to $\hat{\nabla}_\alpha$ as the angular gradient. Furthermore, we define the angular Laplacian operator,

$$\hat{\nabla}^2 = \hat{\nabla}_\alpha \hat{\nabla}^\alpha = \frac{\partial^2}{\partial \theta^2} + \cot \theta \frac{\partial}{\partial \theta} + \frac{1}{\sin^2 \theta} \frac{\partial^2}{\partial \phi^2}. \quad (\text{A.4})$$

Using the angular derivatives of the basis vectors,

$$\begin{aligned} \frac{\partial}{\partial \theta} n^\alpha &= \theta^\alpha, & \frac{\partial}{\partial \theta} \theta^\alpha &= -n^\alpha, & \frac{\partial}{\partial \theta} \phi^\alpha &= 0, \\ \frac{1}{\sin \theta} \frac{\partial}{\partial \phi} n^\alpha &= \phi^\alpha, & \frac{1}{\sin \theta} \frac{\partial}{\partial \phi} \theta^\alpha &= \cot \theta \phi^\alpha, & \frac{1}{\sin \theta} \frac{\partial}{\partial \phi} \phi^\alpha &= -n^\alpha - \cot \theta \theta^\alpha, \end{aligned} \quad (\text{A.5})$$

we can derive the following relations that are used for the calculations in this work. First of all, applying the angular gradient and angular Laplacian to n^α yields

$$\hat{\nabla}_\beta n^\alpha = \theta_\beta \theta^\alpha + \phi_\beta \phi^\alpha = -n_\beta n^\alpha + \delta_\beta^\alpha, \quad \hat{\nabla}^2 n^\alpha = -n^\alpha \hat{\nabla}^\beta n_\beta = -2n^\alpha. \quad (\text{A.6})$$

For calculations involving the shear components, we also need the following identities:

$$\Phi_1^{\alpha\beta} \hat{\nabla}_\alpha = \theta^\beta \frac{\partial}{\partial \theta} - \phi^\beta \frac{1}{\sin \theta} \frac{\partial}{\partial \phi}, \quad \Phi_2^{\alpha\beta} \hat{\nabla}_\alpha = \phi^\beta \frac{\partial}{\partial \theta} + \theta^\beta \frac{1}{\sin \theta} \frac{\partial}{\partial \phi}, \quad (\text{A.7})$$

and

$$\Phi_1^{\alpha\beta} \hat{\nabla}_\alpha \hat{\nabla}_\beta = \frac{\partial^2}{\partial \theta^2} - \cot \theta \frac{\partial}{\partial \theta} - \frac{1}{\sin^2 \theta} \frac{\partial^2}{\partial \phi^2}, \quad \Phi_2^{\alpha\beta} \hat{\nabla}_\alpha \hat{\nabla}_\beta = \frac{\partial}{\partial \theta} \left(\frac{1}{\sin \theta} \frac{\partial}{\partial \phi} \right), \quad (\text{A.8})$$

where Φ_i , for $i = 1, 2$, is defined in equation (2.8). Applied to n^γ , we obtain

$$\Phi_i^{\alpha\beta} \hat{\nabla}_\alpha n^\gamma = \Phi_i^{\beta\gamma}, \quad \Phi_i^{\alpha\beta} \hat{\nabla}_\alpha \hat{\nabla}_\beta n^\gamma = 0. \quad (\text{A.9})$$

We emphasize that the observed angular direction $\hat{\mathbf{n}}$ and the two orthonormal directions $\boldsymbol{\theta}$ and $\boldsymbol{\phi}$ are defined in the observer rest frame only. Thus, the definitions presented here are independent of any FRW coordinates in the space-time manifold.

B Calculating tensor mode contributions using the Limber approximation

In this section, we provide the calculation of the tensor mode contribution to the weak lensing angular power spectra given in section 4. As the Limber approximation described by equations (4.1) and (4.2) is used to obtain these results, we only consider modes with $\mathbf{k} = \mathbf{k}_\perp$, where \mathbf{k}_\perp denotes the projection on the plane orthogonal to the line of sight. For such modes with direction vector $\hat{\mathbf{k}}_\perp = \hat{\mathbf{k}} = (\cos \varphi, \sin \varphi, 0)$, the vectors $e_1(\hat{\mathbf{k}}_\perp)$ and $e_2(\hat{\mathbf{k}}_\perp)$ are given by

$$e_1(\hat{\mathbf{k}}_\perp) = (0, 0, -1), \quad e_2(\hat{\mathbf{k}}_\perp) = (-\sin \varphi, \cos \varphi, 0), \quad (\text{B.1})$$

which yields

$$e_{ij}^+(\hat{\mathbf{k}}_\perp) = \begin{pmatrix} -\sin^2 \varphi & \cos \varphi \sin \varphi & 0 \\ \cos \varphi \sin \varphi & -\cos^2 \varphi & 0 \\ 0 & 0 & 1 \end{pmatrix}, \quad e_{ij}^\times(\hat{\mathbf{k}}_\perp) = \begin{pmatrix} 0 & 0 & \sin \varphi \\ 0 & 0 & -\cos \varphi \\ \sin \varphi & -\cos \varphi & 0 \end{pmatrix}, \quad (\text{B.2})$$

for the polarization tensors. The following relations apply:

$$n^\alpha n^\beta e_{\alpha\beta}^+(\hat{\mathbf{k}}_\perp) = 1, \quad n^\alpha n^\beta e_{\alpha\beta}^\times(\hat{\mathbf{k}}_\perp) = 0, \quad (\text{B.3})$$

$$n^\alpha \hat{k}_\perp^\beta e_{\alpha\beta}^+(\hat{\mathbf{k}}_\perp) = 0, \quad n^\alpha \hat{k}_\perp^\beta e_{\alpha\beta}^\times(\hat{\mathbf{k}}_\perp) = 0, \quad (\text{B.4})$$

$$\Phi_i^{\alpha\beta} e_{\alpha\beta}^+(\hat{\mathbf{k}}_\perp) = \mathcal{A}_i(2\varphi), \quad \Phi_i^{\alpha\beta} e_{\alpha\beta}^\times(\hat{\mathbf{k}}_\perp) = 0, \quad (\text{B.5})$$

$$n^\alpha \Phi_i^{\beta\gamma} \hat{k}_{\perp\gamma} e_{\alpha\beta}^+(\hat{\mathbf{k}}_\perp) = 0, \quad n^\alpha \Phi_i^{\beta\gamma} \hat{k}_{\perp\gamma} e_{\alpha\beta}^\times(\hat{\mathbf{k}}_\perp) = \mathcal{B}_i(2\varphi), \quad (\text{B.6})$$

$$\Phi_i^{\alpha\beta} \hat{k}_{\perp\alpha} \hat{k}_{\perp\beta} = \mathcal{A}_i(2\varphi), \quad (\text{B.7})$$

where $\mathcal{A}_i(\varphi)$ and $\mathcal{B}_i(\varphi)$ are defined as

$$\mathcal{A}_i(\varphi) \equiv \begin{cases} \cos \varphi & \text{for } i = 1, \\ \sin \varphi & \text{for } i = 2. \end{cases}, \quad \mathcal{B}_i(\varphi) \equiv \begin{cases} \sin \varphi & \text{for } i = 1, \\ \cos \varphi & \text{for } i = 2. \end{cases}. \quad (\text{B.8})$$

Using these basic relations, we now compute the tensor mode contribution to the magnification angular power spectrum for some general source distribution function $n(\bar{r})$. First, note that the term containing the angular Laplacian in equations (2.29) can be re-written as

$$\hat{\nabla}^2 C_\parallel = n^\alpha n^\beta \hat{\nabla}^2 C_{\alpha\beta} + 2C_{\parallel\beta} \hat{\nabla}^2 n^\beta + 4n^\alpha \hat{\nabla}_\gamma n^\beta \hat{\nabla}^\gamma C_{\alpha\beta} + 2C_{\alpha\beta} \hat{\nabla}_\gamma n^\alpha \hat{\nabla}^\gamma n^\beta. \quad (\text{B.9})$$

Using equations (A.6) and re-naming indices, this can be further simplified as

$$\hat{\nabla}^2 C_\parallel = n^\alpha n^\beta \hat{\nabla}^2 C_{\alpha\beta} + 4n^\alpha \hat{\nabla}^\beta C_{\alpha\beta} - 2C_\parallel, \quad (\text{B.10})$$

which is, using equation (3.12), in Fourier space given by

$$\mathcal{F} \left[\hat{\nabla}^2 C_\parallel \right] (\mathbf{k}, \bar{r}) = \left(-\bar{r}^2 n^\alpha n^\beta k_\perp^2 + 4i\bar{r} n^\alpha k_\perp^\beta - 2n^\alpha n^\beta \right) \sum_s C_s(\mathbf{k}, \bar{r}) e_{\alpha\beta}^s(\hat{\mathbf{k}}), \quad (\text{B.11})$$

where \mathcal{F} denotes the Fourier transform. Hence, using equations (B.3) and (B.4) and considering only modes with $\mathbf{k}_\perp = \mathbf{k}$, we obtain

$$\mathcal{F} \left[\hat{\nabla}^2 C_\parallel \right] (\mathbf{k}_\perp, \bar{r}) = -(k_\perp^2 \bar{r}^2 + 2)T(\bar{r})C_+(\mathbf{k}_\perp). \quad (\text{B.12})$$

The term containing the angular gradient can be re-written as

$$\hat{\nabla}^\alpha C_{\parallel\alpha} = n^\beta \hat{\nabla}^\alpha C_{\alpha\beta} + C_{\alpha\beta} \hat{\nabla}^\alpha n^\beta = n^\beta \hat{\nabla}^\alpha C_{\alpha\beta} - C_\parallel, \quad (\text{B.13})$$

which is given in Fourier space by

$$\mathcal{F} \left[\hat{\nabla}^\alpha C_{\parallel\alpha} \right] (\mathbf{k}, \bar{r}) = \left(i\bar{r} n^\beta k_\perp^\alpha - n^\alpha n^\beta \right) \sum_s C_s(\mathbf{k}, \bar{r}) e_{\alpha\beta}^s(\hat{\mathbf{k}}). \quad (\text{B.14})$$

Again using equations (B.3) and (B.4), this yields for modes perpendicular to the line of sight:

$$\mathcal{F} \left[\hat{\nabla}^\alpha C_{\parallel\alpha} \right] (\mathbf{k}_\perp, \bar{r}) = -T(k_\perp, \bar{r})C_+(\mathbf{k}_\perp). \quad (\text{B.15})$$

To deal with all other terms appearing in the expression (2.29) for the tensor mode contribution to the magnification, simply note that equation (B.3) yields $\mathcal{F}[C_\parallel](\mathbf{k}_\perp, \bar{r}) = T(k_\perp, \bar{r})C_+(\mathbf{k}_\perp)$. Hence, we obtain for the Fourier transform of expression (2.29),

$$\begin{aligned} \Delta D_t(\mathbf{k}_\perp) &= \int_0^{\bar{r}S} d\bar{r} \left(h(\bar{r}) + g(\bar{r}) - \frac{n(\bar{r})}{2} \right) T(k_\perp, \bar{r})C_+(\mathbf{k}_\perp) + \int_0^{\bar{r}S} d\bar{r} h(\bar{r})T(k_\perp, \bar{r})C_+(\mathbf{k}_\perp) \\ &\quad - \frac{1}{2} \int_0^{\bar{r}S} d\bar{r} g(\bar{r})(k_\perp^2 \bar{r}^2 + 2)T(k_\perp, \bar{r})C_+(\mathbf{k}_\perp) + \int_0^{\bar{r}S} d\bar{r} (h(\bar{r})\bar{r} - q(\bar{r}))T'(k_\perp, \bar{r})C_+(\mathbf{k}_\perp), \end{aligned} \quad (\text{B.16})$$

where we have ignored the observer term as it can not be treated within the Limber approximation. Summing up the contribution from the separate terms, this equation simplifies to

$$\begin{aligned}\Delta D_{\text{t.}}(\mathbf{k}_{\perp}) &= \int_0^{\bar{r}^S} d\bar{r} \left(-\frac{k_{\perp}^2 \bar{r}^2}{2} g(\bar{r}) + 2h(\bar{r}) - \frac{n(\bar{r})}{2} \right) T(k_{\perp}, \bar{r}) C_+(\mathbf{k}_{\perp}) \\ &\quad + \int_0^{\bar{r}^S} d\bar{r} (h(\bar{r})\bar{r} - q(\bar{r})) T'(k_{\perp}, \bar{r}) C_+(\mathbf{k}_{\perp}).\end{aligned}\quad (\text{B.17})$$

Now, applying equation (3.18) and the Limber approximation as described in equation (4.2), equation (4.7) for the tensor mode contribution to the angular power spectrum $C^{\Delta D}(l)$ can be easily obtained. Similarly, the tensor mode contribution to the shear E- and B-modes can be calculated using equations (B.3)–(B.7). However, as concluded in [36] and as we confirm in section 6.1, the Limber approximation is in fact not applicable to tensor modes at any scales. Therefore, we leave out the details for this calculation and simply state the result in equation (4.19).

C Contribution of different \mathbf{k} -vectors to the angular power spectrum

Given a scalar quantity $A(\hat{\mathbf{n}})$, such as the magnification or the spin-raised and -lowered shear components, the resulting angular power spectrum is given by

$$C^A(l) = \left\langle a_{lm}^A (a_{lm}^A)^* \right\rangle = \int \int \frac{d^3k}{(2\pi)^3} \frac{d^3k'}{(2\pi)^3} \left\langle a_{lm}^A(\mathbf{k}) (a_{lm}^A(\mathbf{k}'))^* \right\rangle = \int \frac{d^3k}{(2\pi)^3} |\tilde{a}_{lm}^A(\mathbf{k})|^2 P_{\zeta}(k), \quad (\text{C.1})$$

where $a_{lm}^A(\mathbf{k})$ is defined in equation (5.5), and we additionally introduced $\tilde{a}_{lm}^A(\mathbf{k})$ as $\tilde{a}_{lm}^A(\mathbf{k}) \equiv \tilde{a}_{lm}^A(\mathbf{k})\zeta(\mathbf{k})$. Thus, $C^A(l)$ needs to be calculated from the contribution of all \mathbf{k} at all angular directions. However, in our calculations in section 5 for the shear components and the magnification, we have only calculated $a_{lm}(\mathbf{k})$ for a k -vector aligned with the z -axis, $\mathbf{k} = k\mathbf{e}_z$, and assumed that this is sufficient to evaluate the resulting angular power spectra. Here, we justify this assumption. Note that in equation (C.1), we assumed that $A(\mathbf{n})$ has only scalar mode contributions, $A(\mathbf{n}) = A^{\text{sc.}}(\mathbf{n})$. However, as we comment below, the arguments in this section also apply to tensor modes.

Let \mathbf{k} be some arbitrary wave-vector, and let \mathbf{n}_1 and \mathbf{n}_2 specify two angular directions. First, note that for any rotation matrix \mathcal{R} , the relation

$$\tilde{A}(\mathbf{k}, \mathbf{n}_1) \tilde{A}^*(\mathbf{k}, \mathbf{n}_2) = \tilde{A}(\mathcal{R}\mathbf{k}, \mathcal{R}\mathbf{n}_1) \tilde{A}^*(\mathcal{R}\mathbf{k}, \mathcal{R}\mathbf{n}_2), \quad (\text{C.2})$$

applies, where $A(\mathbf{k}, \mathbf{n}) \equiv \tilde{A}(\mathbf{k}, \mathbf{n})\zeta(\mathbf{k})$. This is based on the fact that the dependence of $\tilde{A}(\mathbf{k}, \mathbf{n})$ can be expressed as a dependence on k and the angle $\mathbf{k} \cdot \mathbf{n}$, which stays invariant when applying the same rotation to both vectors. Now, defining $\mathbf{k} \equiv \mathcal{R}_k \mathbf{e}_z$, $\mathbf{n}_1 \equiv \mathcal{R}_k \mathbf{n}'_1$ and $\mathbf{n}_2 \equiv \mathcal{R}_k \mathbf{n}'_2$, we obtain

$$\begin{aligned}\sum_m |\tilde{a}_{lm}^A(\mathbf{k})|^2 &= \sum_m \int d\Omega_1 \int d\Omega_2 \tilde{A}(\mathbf{k}, \mathbf{n}_1) \tilde{A}^*(\mathbf{k}, \mathbf{n}_2) Y_{lm}(\mathbf{n}_1) Y_{lm}^*(\mathbf{n}_2) \\ &= \sum_m \int d\Omega'_1 \int d\Omega'_2 \tilde{A}(\mathbf{k}, \mathcal{R}_k \mathbf{n}'_1) \tilde{A}^*(\mathbf{k}, \mathcal{R}_k \mathbf{n}'_2) Y_{lm}(\mathcal{R}_k \mathbf{n}'_1) Y_{lm}^*(\mathcal{R}_k \mathbf{n}'_2) \\ &= \sum_m \int d\Omega'_1 \int d\Omega'_2 \tilde{A}(k\mathbf{e}_z, \mathbf{n}'_1) \tilde{A}^*(k\mathbf{e}_z, \mathbf{n}'_2) Y_{lm}(\mathcal{R}_k \mathbf{n}'_1) Y_{lm}^*(\mathcal{R}_k \mathbf{n}'_2),\end{aligned}\quad (\text{C.3})$$

where we have performed a change of variables in the second line, and used equation (C.2) in the third line. By applying the addition theorem of spherical harmonics,

$$\sum_m Y_{lm}(\mathbf{n}_1) Y_{lm}^*(\mathbf{n}_2) = \frac{2l+1}{4\pi} P_l(\mathbf{n}_1 \cdot \mathbf{n}_2) = \sum_m Y_{lm}(\mathcal{R}\mathbf{n}_1) Y_{lm}^*(\mathcal{R}\mathbf{n}_2), \quad (\text{C.4})$$

we can further express this result as

$$\sum_m |\tilde{a}_{lm}^A(\mathbf{k})|^2 = \sum_m \int d\Omega'_1 \int d\Omega'_2 \tilde{A}(k\mathbf{e}_z, \mathbf{n}'_1) \tilde{A}^*(k\mathbf{e}_z, \mathbf{n}'_2) Y_{lm}(\mathbf{n}'_1) Y_{lm}^*(\mathbf{n}'_2) = \sum_m |\tilde{a}_{lm}^A(k\mathbf{e}_z)|^2. \quad (\text{C.5})$$

Finally, noting that $C^A(l)$ is independent of m , we can rewrite equation (C.1) as

$$C^A(l) = \frac{1}{2l+1} \int \frac{d^3k}{(2\pi)^3} \sum_m |\tilde{a}_{lm}^A(\mathbf{k})|^2 P_\zeta(k) = \frac{1}{2l+1} \int \frac{d^3k}{(2\pi)^3} \sum_m |\tilde{a}_{lm}^A(k\mathbf{e}_z)|^2 P_\zeta(k), \quad (\text{C.6})$$

proving that, indeed, we can calculate $C^A(l)$ from the contribution of k -vectors aligned with the z -axis only. Note that, while $\langle a_{lm}^A (a_{lm}^A)^* \rangle$ is equal for all m due to statistical isotropy, this does not apply for the contribution of a single k -mode. In particular, a k -mode aligned with the z -axis contributes only to $m=0$ (for a pure scalar mode contribution), while this would not be true for a general k -mode since $a_{lm}^A(\mathbf{k}) \neq a_{lm}^A(k\mathbf{e}_z)$ in general. Indeed, the summation over m is vital in our calculation, as it allows us to apply the addition theorem in equation (C.4) to obtain equation (C.5). Only after replacing the general k -mode with one aligned with the line of sight, $\mathbf{k} = k\mathbf{e}_z$, the summation over m can be dropped and replaced by the contribution of $m=0$.

Finally, note that all arguments in this section also apply to the contribution of tensor modes, described by $a_{lm}^{A.t.}$. In that case, we define

$$a_{lm}^{A.t.}(\mathbf{k}) = \sum_{p=\pm 1} \tilde{a}_{lm,p}^{A.t.}(\mathbf{k}) C_p(k), \quad A^t(\mathbf{k}, \mathbf{n}) = \sum_{p=\pm 1} \tilde{A}_p^t(\mathbf{k}, \mathbf{n}) C_p(k), \quad (\text{C.7})$$

and repeat the calculations in (C.2)–(C.5), replacing $\tilde{a}_{lm}^A(\mathbf{k})$ and $\tilde{A}(\mathbf{k}, \mathbf{n})$ by $\tilde{a}_{lm,p}^{A.t.}(\mathbf{k})$ and $\tilde{A}_p^t(\mathbf{k}, \mathbf{n})$. Then, we obtain the expression

$$\begin{aligned} C^A(l) &= \frac{1}{16(2l+1)} \int \frac{d^3k}{(2\pi)^3} \sum_{p=\pm 1} \sum_m |\tilde{a}_{lm,p}^{A.t.}(\mathbf{k})|^2 P_T(k) \\ &= \frac{1}{16(2l+1)} \int \frac{d^3k}{(2\pi)^3} \sum_{p=\pm 1} \sum_m |\tilde{a}_{lm,p}^{A.t.}(k\mathbf{e}_z)|^2 P_T(k), \end{aligned} \quad (\text{C.8})$$

where the summation over m in the second line can be replaced by the contribution of $m=2$ for $p=1$, and $m=-2$ for $p=-1$.

D Detailed calculation of the spin-2 shear components $_{\pm 2}\gamma(\mathbf{k}, \mathbf{n})$

Here, we describe how the expressions for $_{\pm 2}\gamma(\mathbf{k}, \mathbf{n})$ given by equations (5.37) and (5.38)–(5.41) are calculated. For ease of notation, we define spin-1 differential operators $\hat{\nabla}_\pm$ as

$$\hat{\nabla}_\pm \equiv m_{\mp}^\alpha \hat{\nabla}_\alpha = \frac{1}{\sqrt{2}} \left(\frac{\partial}{\partial \theta} \pm i \frac{1}{\sin \theta} \frac{\partial}{\partial \phi} \right). \quad (\text{D.1})$$

Before turning to the calculation of $_{\pm 2}\gamma(\mathbf{k}, \mathbf{n})$, we first derive several useful relations involving the operator $\hat{\nabla}_{\pm}$ and the spin-1 basis m_{\pm}^{α} as a preliminary work. Throughout this section, we assume that the Fourier mode \mathbf{k} is aligned with the positive z -direction, i.e. with unit vector $\hat{\mathbf{k}} = (0, 0, 1)$. With this assumption, we obtain the product

$$\mathbf{m}_{\pm} \cdot \mathbf{k} = -\frac{k\sqrt{1-\mu^2}}{\sqrt{2}}, \quad (\text{D.2})$$

and, following the definitions given in equation (3.13),

$$e_{\alpha\beta}^{+} = \begin{pmatrix} 1 & 0 & 0 \\ 0 & -1 & 0 \\ 0 & 0 & 0 \end{pmatrix}, \quad e_{\alpha\beta}^{\times} = \begin{pmatrix} 0 & 1 & 0 \\ 1 & 0 & 0 \\ 0 & 0 & 0 \end{pmatrix}, \quad e_{\alpha\beta}^{\text{p}} = \begin{pmatrix} 1 & i\text{p} & 0 \\ i\text{p} & -1 & 0 \\ 0 & 0 & 0 \end{pmatrix}, \quad (\text{D.3})$$

which allows us to easily derive the relations

$$e_{\alpha\beta}^{\text{p}} n^{\alpha} m_{\pm}^{\beta} = \frac{\sqrt{1-\mu^2}(\mu \pm \text{p})}{\sqrt{2}} e^{ip2\phi}, \quad (\text{D.4})$$

$$e_{\alpha\beta}^{\text{p}} m_{\pm}^{\alpha} m_{\pm}^{\beta} = \frac{1}{2}(\mu \pm \text{p})^2 e^{ip2\phi}, \quad (\text{D.5})$$

$$e_{\alpha\beta}^{\text{p}} n^{\alpha} n^{\beta} = (1 - \mu^2) e^{ip2\phi}, \quad (\text{D.6})$$

where $\text{p} = \pm 1$. Now, applying equation (A.5), we can derive the basic relations

$$\hat{\nabla}_{\pm} n^{\alpha} = m_{\pm}^{\alpha}, \quad \hat{\nabla}_{\pm} m_{\pm}^{\alpha} = \frac{\mu}{\sqrt{2(1-\mu^2)}} m_{\pm}^{\alpha}, \quad \hat{\nabla}_{\pm}^2 n^{\alpha} = \frac{\mu}{\sqrt{2(1-\mu^2)}} m_{\pm}^{\alpha}. \quad (\text{D.7})$$

which we use to calculate

$$\hat{\nabla}_{\pm} e^{i\bar{r}\mathbf{k}\cdot\mathbf{n}} = i\bar{r} e^{i\bar{r}\mathbf{k}\cdot\mathbf{n}} (\hat{\nabla}_{\pm} \mathbf{n}) \cdot \mathbf{k} = i\bar{r} \mathbf{m}_{\pm} \cdot \mathbf{k} e^{i\bar{r}\mathbf{k}\cdot\mathbf{n}} = -i \frac{k\bar{r}\sqrt{1-\mu^2}}{\sqrt{2}} e^{i\bar{r}\mathbf{k}\cdot\mathbf{n}}, \quad (\text{D.8})$$

$$m_{\pm}^{\alpha} m_{\pm}^{\beta} \hat{\nabla}_{\alpha} \hat{\nabla}_{\beta} = \hat{\nabla}_{\pm}^2 - (\hat{\nabla}_{\pm} m_{\pm}^{\beta}) \hat{\nabla}_{\beta} = \hat{\nabla}_{\pm}^2 - \frac{\mu}{\sqrt{2(1-\mu^2)}} \hat{\nabla}_{\pm}, \quad (\text{D.9})$$

$$\hat{\nabla}_{\pm}^2 e^{i\bar{r}\mathbf{k}\cdot\mathbf{n}} = i\bar{r} (\hat{\nabla}_{\pm} \mathbf{m}_{\pm}) \cdot \mathbf{k} e^{i\bar{r}\mathbf{k}\cdot\mathbf{n}} - \bar{r}^2 (\mathbf{m}_{\pm} \cdot \mathbf{k})^2 e^{i\bar{r}\mathbf{k}\cdot\mathbf{n}} = -i \frac{\mu k \bar{r}}{2} e^{i\bar{r}\mathbf{k}\cdot\mathbf{n}} - \frac{k^2 \bar{r}^2 (1-\mu^2)}{2} e^{i\bar{r}\mathbf{k}\cdot\mathbf{n}}. \quad (\text{D.10})$$

From this, it further follows that

$$m_{\pm}^{\alpha} m_{\pm}^{\beta} \hat{\nabla}_{\alpha} \hat{\nabla}_{\beta} e^{i\bar{r}\mathbf{k}\cdot\mathbf{n}} = -\frac{k^2 \bar{r}^2 (1-\mu^2)}{2} e^{i\bar{r}\mathbf{k}\cdot\mathbf{n}}. \quad (\text{D.11})$$

Having derived these relations, let us now look at the scalar term, $_{\pm 2}\text{S}(\mathbf{n})$ given in equation (5.34). Writing $\Psi(\mathbf{n}, \bar{r})$ as the Fourier transform of $\Psi(\mathbf{k}, \bar{r})$ and changing the order of integration, we obtain

$$_{\pm 2}\text{S}(\mathbf{n}) = \int \frac{d^3\mathbf{k}}{(2\pi)^3} \int_0^{\bar{r}_s} d\bar{r} \left(\frac{\bar{r}_s - \bar{r}}{\bar{r}_s \bar{r}} \right) 2\Psi(\mathbf{k}, \bar{r}) m_{\mp}^{\alpha} m_{\mp}^{\beta} \hat{\nabla}_{\alpha} \hat{\nabla}_{\beta} e^{i\bar{r}\mathbf{k}\cdot\mathbf{n}}. \quad (\text{D.12})$$

From this, together with equation (D.11), the expression for $_{\pm 2}\text{S}(\mathbf{n}, \mathbf{k})$ given in equation (5.37) follows.

Next, we consider the tensor terms given in equation (5.35), for which we need to recall that we can write $C_{\alpha\beta}(\mathbf{n}, \bar{r})$ as

$$C_{\alpha\beta}(\mathbf{n}, \bar{r}) = \int \frac{d^3\mathbf{k}}{(2\pi)^3} \sum_{\mathbf{p}} e_{\alpha\beta}^{\mathbf{p}}(\hat{\mathbf{k}}) C_{\mathbf{p}}(\mathbf{k}, \bar{r}). \quad (\text{D.13})$$

Applying this and equation (D.5), the expressions for ${}_{\pm 2}\text{T0}(\mathbf{k}, \mathbf{n})$ and ${}_{\pm 2}\text{T3}(\mathbf{k}, \mathbf{n})$ given in equations (5.38) and (5.41) follow easily. For ${}_{\pm 2}\text{T1}(\mathbf{k}, \mathbf{n})$, replacing $C_{\alpha\beta}(\mathbf{n}, \bar{r})$ as above yields an equation involving the expression

$$\begin{aligned} e_{\gamma\delta}^{\mathbf{p}} m_{\mp}^{\alpha} m_{\mp}^{\beta} \hat{\nabla}_{\alpha} \hat{\nabla}_{\beta} \left(n^{\gamma} n^{\delta} e^{i\bar{r}\mathbf{k}\cdot\mathbf{n}} \right) &= e_{\gamma\delta}^{\mathbf{p}} \left[2n^{\delta} e^{i\bar{r}\mathbf{k}\cdot\mathbf{n}} \hat{\nabla}_{\mp}^2 n^{\gamma} + n^{\gamma} n^{\delta} \hat{\nabla}_{\mp}^2 e^{i\bar{r}\mathbf{k}\cdot\mathbf{n}} + 2e^{i\bar{r}\mathbf{k}\cdot\mathbf{n}} \hat{\nabla}_{\mp} n^{\gamma} \hat{\nabla}_{\mp} n^{\delta} \right. \\ &\quad \left. + 4n^{\gamma} \hat{\nabla}_{\mp} n^{\delta} \hat{\nabla}_{\mp} e^{i\bar{r}\mathbf{k}\cdot\mathbf{n}} - n^{\gamma} \frac{\mu}{\sqrt{2(1-\mu^2)}} \left(2e^{i\bar{r}\mathbf{k}\cdot\mathbf{n}} \hat{\nabla}_{\mp} n^{\delta} + n^{\delta} \hat{\nabla}_{\mp} e^{i\bar{r}\mathbf{k}\cdot\mathbf{n}} \right) \right], \end{aligned} \quad (\text{D.14})$$

where we have used equation (D.9). Now, by applying equations (D.7), (D.8) and (D.10) and also (D.4)–(D.6), we can further rewrite this expression as

$$e_{\gamma\delta}^{\mathbf{p}} m_{\mp}^{\alpha} m_{\mp}^{\beta} \hat{\nabla}_{\alpha} \hat{\nabla}_{\beta} \left(n^{\gamma} n^{\delta} e^{i\bar{r}\mathbf{k}\cdot\mathbf{n}} \right) = \left[(\mu \mp p)^2 - \frac{k^2 \bar{r}^2 (1 - \mu^2)^2}{2} - i2k\bar{r}(1 - \mu^2)(\mu \mp p) \right] e^{ip2\phi} e^{i\bar{r}\mathbf{k}\cdot\mathbf{n}}, \quad (\text{D.15})$$

and the equation (5.39) for ${}_{\pm 2}\text{T1}(\mathbf{k}, \mathbf{n})$ follows. Finally, we need to repeat the calculation for the term ${}_{\pm 2}\text{T2}(\mathbf{n})$, which involves the expression

$$e_{\alpha\gamma}^{\mathbf{p}} m_{\mp}^{\alpha} \hat{\nabla}_{\mp} \left(n^{\gamma} e^{i\bar{r}\mathbf{k}\cdot\mathbf{n}} \right) = \left[-\frac{ik\bar{r}}{2} (1 - \mu^2)(\mu \mp p) + \frac{1}{2} (\mu \mp p)^2 \right] e^{ip2\phi} e^{i\bar{r}\mathbf{k}\cdot\mathbf{n}}, \quad (\text{D.16})$$

where we have used equations (D.7) and (D.8) along with equations (D.4) and (D.5). This proves the expression for ${}_{\pm 2}\text{T2}(\mathbf{k}, \mathbf{n})$ given in equation (5.40).

References

- [1] LSST collaboration, C.W. Stubbs, D. Sweeney, J.A. Tyson, *Bull. Astron. Math. Soc.* **36** (2004) 108.
- [2] J. Green et al. (2012), [arXiv:1208.4012](#).
- [3] Euclid collaboration, R. Laureijs et al. (2011), [arXiv:1110.3193](#).
- [4] L. Amendola et al., *Living Rev. Relativity* **16** (2013) 6, [arXiv:1206.1225](#).
- [5] K. Kuijken et al., *Mon. Not. Roy. Astron. Soc.* **454** (2015) 3500, [arXiv:1507.00738](#).
- [6] R. Mandelbaum (2017), [arXiv:1710.03235](#).
- [7] N. Kaiser, *Astrophys. J.* **388** (1992) 272.
- [8] T. D. Kitching et al., *Mon. Not. R. Astron. Soc.* **469** (2017) 2737, [arXiv:1611.04954](#).
- [9] F. Bernardeau, C. Bonvin, N. Van de Rijdt and F. Vernizzi, *Phys. Rev. D* **86** (2012) 023001, [arXiv:1112.4430](#).
- [10] M. Kilbinger et al., *Mon. Not. R. Astron. Soc.* **472** (2017) 2126, [arXiv:1702.05301](#).
- [11] M. LoVerde and N. Afshordi, *Phys. Rev. D* **78** (2008) 123506, [arXiv:0809.5112](#).
- [12] P. Lemos, A. Challinor and G. Efstathiou, *JCAP* **05** (2017) 014, [arXiv:1704.01054](#).

- [13] J. Yoo et al., JCAP **04** (2018) 029, [arXiv:1802.03403](#).
- [14] F. Schmidt and D. Jeong, Phys. Rev. D **86** (2012) 083527, [arXiv:1204.3625](#).
- [15] N. Grimm and J. Yoo, JCAP **07** (2018) 067, [arXiv:1806.00017](#).
- [16] J. Alsing, D. Kirk, A. Heavens and A. Jaffe, Mon. Not. Roy. Astron. Soc. **452** no.2 (2015) 1202, [arXiv:1410.7839](#).
- [17] F. Schmidt et al., Astrophys. J. **744** (2012) L22, [arXiv:1111.3679](#).
- [18] B. Casaponsa et al., Mon. Not. Roy. Astron. Soc. **430** (2013) 2844, [arXiv:1209.1646](#).
- [19] M. Bartelmann and P. Schneider, Phys. Rept. **340** (2001) 291, [arXiv:astro-ph/9912508](#).
- [20] G. V. Skrotsky, Dokl. Akad. Nauk SSSR **114** (1957) 73.
- [21] C. Bonvin, R. Durrer and M. A. Gasparini, Phys. Rev. D **73** (2006) 023523 [erratum: Phys. Rev. D **85** 029901 (2012)], [arXiv:astro-ph/0511183](#).
- [22] J. Yoo and F. Scaccabarozzi, JCAP **09** (2016) 046, [arXiv:1606.08453](#).
- [23] S. Biern and J. Yoo, JCAP **04** (2016) 045, [arXiv:1606.01910](#).
- [24] M. Kilbinger, Rep. Prog. Phys. **78** (2015) 086901, [arXiv:1411.0115](#).
- [25] D. Blas, J. Lesgourgues and T. Tram, JCAP **07** (2011) 034, [arXiv:1104.2933](#).
- [26] M. C. Guzzetti, N. Bartolo, M. Liguori and S. Matarrese, Riv. Nuovo Cim. **39** no.9 (2016) 399, [arXiv:1605.01615](#).
- [27] M. Shirasaki, *Probing Cosmic Dark Matter and Dark Energy with Weak Gravitational Lensing Statistics*, Springer (2016).
- [28] R. Arnowitt, S. Deser and C. W. Misner, “Gravitation: an introduction to current research” edited Louis Witten ed. (Wiley 1962), chapter 7, pp 227–265, [arXiv:gr-qc/0405109](#).
- [29] H. Noh and J. Hwang, Phys. Rev. D **69** (2004) 104011, [arXiv:astro-ph/0305123](#).
- [30] J. Yoo and J. O. Gong, JCAP **07** (2016) 017, [arXiv:1602.06300](#).
- [31] W. Hu and M. White, Phys. Rev. D **56** (1997) 596, [astro-ph/9702170](#).
- [32] F. Schmidt and D. Jeong, Phys. Rev. D **86** (2012) 083513, [arXiv:1205.1514](#).
- [33] A. Stebbins (1996), [astro-ph/9609149](#).
- [34] Planck Collaboration, N. Aghanim et al., Astron. Astrophys. **641** (2020) A6, [arXiv:1807.06209](#).
- [35] Planck Collaboration, Y. Akrami et al., Astron. Astrophys. **641** (2020) A10, [arXiv:1807.06211](#).
- [36] F. Schmidt and D. Jeong, Phys. Rev. D **86** (2012) 083512, [arXiv:1205.1512](#).